GPR Propagation Simulation and Fat Dipole Antenna Design

Tai-Lin Greg Chen

A dissertation submitted to the Department of Electrical Engineering,
University of Cape Town, in fulfilment of the requirements
for the degree of Master of Science in Engineering.

Cape Town, March 2006

Declaration

I declare that this dissertation is my own, unaided work. It is being submitted for the degree of Master of Science in Engineering in the University of Cape Town. It has not been submitted before for any degree or examination in any other university.

Signature of Author .....

Cape Town

February 2006

Abstract

Two applications of FEKO are reported. The first application is investigating how antennas propagate, reflect, and the difference in transmit and receive signals in various ground media. Results of the ground penetration simulations done in FEKO (MoM- Method of Moment) is compared to Finite Difference Time Domain (FDTD) results simulated by Mukhopadhyay with the same physical model.

The second application is to model and fabricate an ultra wide-band antenna with implementation of the fat dipole design. The design considerations applied to improve antenna performance include antenna feed configurations, substrate width, aperture dimension, cavity implementation, terminating resistance, antenna impedance and balun matching. After the design process was completed, fabrication of the antenna took place and the design validated.

Acknowledgements

I would like to thank my supervisor, Prof. Mike Inggs for his guidance, encouragement and motivation throughout the entire research period. Special thanks goes to my family and friends whose continuous support was invaluable to the completion of this project.

I would also like to thank EM Software & Systems for the FEKO licences provided to me, as well as Pradip Mukhopadhyay, Dr. Richard Lord, the RRSG staff and all my colleagues in the RRSG for their contribution towards the research.

Contents

List of Figures

List of Tables

List of Symbols

σ	—	Electrical conductivity
ϵ_r	—	Relative dielectric permittivity
c	—	Speed of light
μ_r	—	Relative dielectric permeability
f_b	—	Operating bandwidth
f_c	—	Centre frequency
f_L	—	Bandwidth starting frequency
f_H	—	Bandwidth ending frequency
Γ	—	Voltage reflective coefficient
Z_L	—	Load Impedance
Z_o	—	Antenna Characteristic Impedance
η	—	Radiation efficiency
G_d	—	Directive Gain
G_p	—	Power Gain
P_{max}	—	Maximum power density
P_t	—	Total power radiated
P_o	—	Total power accepted
λ	—	Wavelength
S11	—	Return loss
S12	—	Insertion loss

Nomenclature

Co-polarization—The polarisation which the antenna is intended to radiate.

Cross-polarization—The polarization orthogonal to a specific reference polarization.

MoM—Method of Moment.

FDTD—Finite Difference Time Domain.

GPR—Ground penetrating radar.

UWB—Ultra wide-band.

NB—Narrow band

KERI—Korea Electro-technology Research Institute

VSWR—Voltage standing wave ratio.

EM—Electromagnetic.

FFT—Fast Fourier transform.

Tx—Transmitter.

Rx—Receiver.

Chapter 1

Introduction

1.1 Project Background

FEKO is a full wave, MoM (method of moment) based simulation software for the analysis of electromagnetic problems such as coupling, antenna design, antenna placement analysis, microstrip design, scattering analysis, etc. It has the ability to solve electrically large problems using accurate full wave techniques. Electromagnetic fields are obtained by first calculating the electric surface currents on conducting surfaces and equivalent electric and magnetic surface current on the surface of a dielectric solid. The currents are calculated using a linear combination of basis functions, where the coefficients are obtained by solving a system of linear equations. Once the current distribution is known, further parameters can be obtained, such as near field, far field, directivity, input impedance of an antenna and importantly, radar cross sections[6].

RRSG (Radar and Remote Sensing Group) at UCT sees this as an opportunity to use FEKO as a modelling tool used in investigating subsurface transmitter-receiver wave response and the design of an ultra wide-band ground penetrating antenna.

1.2 Ground Penetrating Radar

Ground penetrating radar (GPR) is a surveying tool that is used to read cross-sectional subsurface information without physically probing or changing the physical form of the medium under investigation. Its main functions are to evaluate the location and depth of subsurface objects and to investigate their presence.

GPR operates by transmitting frequency waves directing down into the ground via a wide-band antenna. When the transmitted signal enters the ground and reaches objects or

mediums with different electrical and dielectric properties, part of the signal is reflected off. This reflected energy is then sensed by the receiver antenna[19].

The following are a list of GPR applications:

- Land mine detection
- Imaging underground caves
- Locating mine tunnels
- Detection of pipes
- Detection of buried debris
- Borehole monostatic, bistatic radar applications

The radar waves can penetrate up to 30 metres[1] depending on the conductivity of the ground and the operating frequency of the antenna. The higher the frequency the better the resolution, but less penetrating depth. The lower the frequency the further the waves can penetrate, but at poorer resolution. In this project, we are interested in designing GPR antennas operating in the region of 400 - 800MHz[1].

1.3 GPR Antenna Requirements

The following antenna specifications were required for this project as well as general GPR practice.

1. Operating bandwidth of between 400 - 800MHz, i.e. Ultra wide-bandwidth, bandwidth greater than 20% of centre frequency.
2. Directive antenna with maximum energy projecting into the ground.
3. Antenna will need to be robust and mobile for active GPR testing.
4. Antenna's input impedance will have to be balanced and transformed to 50Ω to minimise mismatch between antenna and radar.

1.4 Project Objectives

The project had two phases which extensively used FEKO as the main source of development. The first phase is learning how to use the package for GPR applications (FEKO's planar multilayer Green's function is an effective tool used to simulate multiple layered media for both antenna design and subsurface detection). First phase of the project is investigating how antennas propagate from the transmiter to a receiver in a multi-layered subsurface environment. The direct and reflected receiver time response signal effected by various ground media is studied. Results of the ground penetration simulations done in FEKO (MoM- Method of Moment) is compared to Finite Difference Time Domain (FDTD) results simulated by Mukhopadhyay with the same physical model. This is shown in Chapter 3.

The second phase is to model and fabricate an ultra wide-band antenna with implementation of the fat dipole design. The results shown in Chapter 4 indicate design considerations applied to improve antenna performance include antenna feed configurations, substrate width, aperture dimension, terminating resistance, antenna impedance and balun matching. After the design process was completed, fabrication of the antenna took place and necessary results were obtained to validate the design.

The project objectives are thus listed below:

1. To familiarise using FEKO and understand the FEKO simulation package in the GPR antenna design and application aspects.
2. To create and simulate the subsurface media models investigated by K.P. Mukhopadhyay using FDTD method in FEKO.
3. Compare the time-domain MoM results with the existing FDTD results.
4. To review the UWB GPR antennas fat dipole antenna design under consideration and simulate for result consistency.
5. Use FEKO to model and improve performance and characteristic of the antenna to meet GPR specifications.
6. To fabricate the antenna and make measurements to validate design.
7. To draw conclusions and make recommendations about the research done in both subsurface media investigation and UWB fat dipole antenna.

1.5 Plan of Development

Chapter 2 reviews the background technologies that are used this in project so far. Simulation methods are explained in this chapter include MoM, Green's function, FDTD and window functions. Antenna definitions such as UWB, reflection coefficient, VSWR, radiation patterns, termination resistance and antenna coupling are also briefly explained.

In Chapter 3, FEKO is used to compare results of transmitter-receiver time response obtained from a finite difference time domain (FDTD) method simulator with those calculated with FEKO. A transmitter and receiver antenna are positioned a set of distances apart situated in a subsurface layered media (sand and clay), time response of the direct and reflected EM waves propagating through the media, and the comparison in shape difference of waveforms obtained between point source (Blackman-Harris window function) and simulated dipole antennas are investigated. [Figure 1.1]

Electrical Property	Sand	Clay
Electrical conductivity, σ [S/m]	0.0001	0.5
Relative dielectric permittivity, ϵ_r	20	40
Relative magnetic permeability. μ_r	1	1

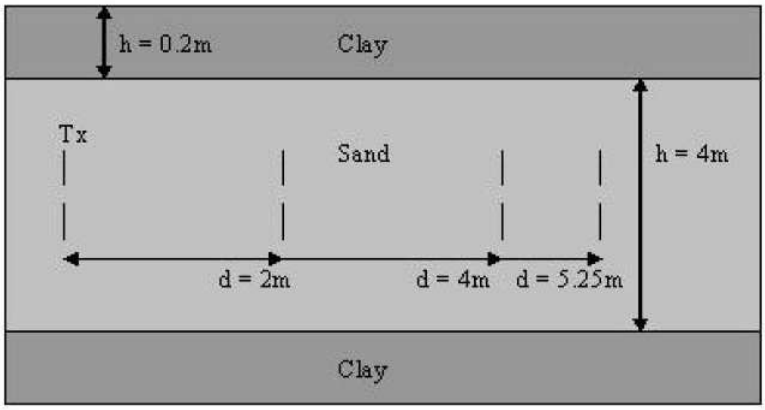

Figure 1.1: Subsurface media simulation configuration

In Chapter 4, a 100-400MHz UWB fat dipole antenna designed by Korea Electro-technology Research Institute (KERI) and Microline Co. Ltd. is reviewed. This design implements the wide-band characteristics of an extended width patch dipole for GPR applications. FEKO is used to model this antenna design and compare the simulated results with the original developer's VSWR (voltage standing wave ratio). The result from this experiment validate the feasibility of modelling such design in FEKO for this project.

After validation of the fat dipole design, several 400-800MHz dipoles were simulated with different dielectric (polystyrene foam) and substrate height to investigate how it effects the

bandwidth, radiated power, electric near field and radiation pattern. This is done to find the best suited antenna for fabrication and testing. Out of the$\lambda/4$,$\lambda/8$,$\lambda/16$ and $\lambda/32$ substrate heights, it was determined that $\lambda/8$ is the best fit with regards to our antenna requirements.

With the GPR specifications in mind, an improved model is created using a Teflon dielectric layer on the bottom of the aperture to protect the antenna from the ground (Real ground will not be flat, hence a strong, non-conductive material is needed for protection from abrasion). A cavity type design is also implemented to maximise the energy directed into the ground, this also provides conductive ground for connecting edge terminating resistance to the aperture. The function of these resistors are to improve the antenna bandwidth as reflections from the lower frequencies are terminated, hence ringing effects will also be reduced. Results such as return loss, VSWR, impedance, directivity, gain, electric near field and radiation efficiency are considered and discussed. [Figure 1.2]

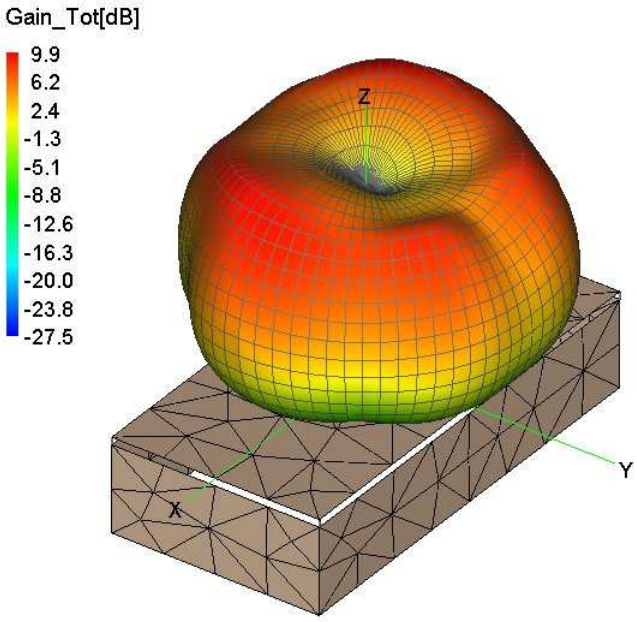

Figure 1.2: Fat dipole ultra wide-band antenna model (3D gain).

In Chapter 5, the construction and testing methods of the antenna are shown and discussed. The results obtained from the network analyser validate the design modelled with FEKO. Besides simulation validation, coupling analysis is also conducted to investigate which Tx and Rx antenna placement configuration will have the least cross-talk.

Chapter 6 contains the conclusions drawn from the comparison done in Chapter 3 and 4. From the ground penetration time response comparison between MoM and FDTD, FEKO's simulation results shows that the MoM's ability to compute transit time in subsurface

layered media has a comparable accuracy to one using FDTD method. FEKO's planar multilayer Green's function has proven to be a useful tool for dielectric antenna modelling, with relatively comparable result with the ones obtained by the network analyser. The modification of implementing an expanded polystyrene filled metal cavity and termination resistors has improved the performance of the system considerably, mainly with regards to radiation efficiency and bandwidth.

Chapter 2

Background Technology

This chapter contains basic definitions of the technologies implemented so far in this project. It will go through the mathematical models used by the EM simulators, and antenna theories involved in this report.

2.1 Method of Moment (MoM)

This is a technique to construct estimators of the parameters that is based on matching the sample moment with the corresponding distribution moments. The fundamental concept behind the MoM is implementing orthogonal expansions and linear algebra to reduce the integral equation problem to a system of simultaneous linear equations. This is achieved by defining the unknown current distribution in terms of an othogonal set of basis functions and defining the boundary conditions[15]. Applying this definition to antenna modelling, it means that the method of moment starts by deriving the current on each segment, or the strength of each moment, by using a coupling Green's function. Green's functions incorporates electrostatic coupling between the moments for if the spatial charge of the currents is known accurately then one can compute the build up of charges at points on the structure. Once the current distribution is known, parameters then can be obtained[6][15].

2.2 Finite-Difference Time Domain (FDTD)

FDTD is a full-wave, dynamic and powerful tool to solve Maxwell's equations. This method belongs in the general class of differential time domain numerical modeling methods. Maxwell's equation are modified to central-difference equations and implemented in software. These equations are solved by solving the electric field at a given instant in

time, then the magnetic field are solved at the next instant in time, and the process repeat itself untill the model is resolved.

FDTD is a useful numerical method suitable for modelling EM wave propagation trough complex media. Furthermore, it is ideal for modelling transient EM fields in inhomogeneous media, such as complex geographical structures as it fit relatively into the finite-difference grid, and absorbing boundary conditions can truncated the grid to simulate an infinite region [8].

2.3 Window Functions

Windowing is a technique used to shape the time-domain information of your measurement data. This is used to minimise spectral leakage in the Fast Fourier Transform (FFT) caused by the edge effect. By applying window functions correctly, side lobes can be greatly reduced with the trade off of having a decreased spectral resolution. The narrowest window in the time-domain will have the widest main lobes in the frequency-domain, and vice-versa. Figure 2.1 shows some of the most common window functions[4].

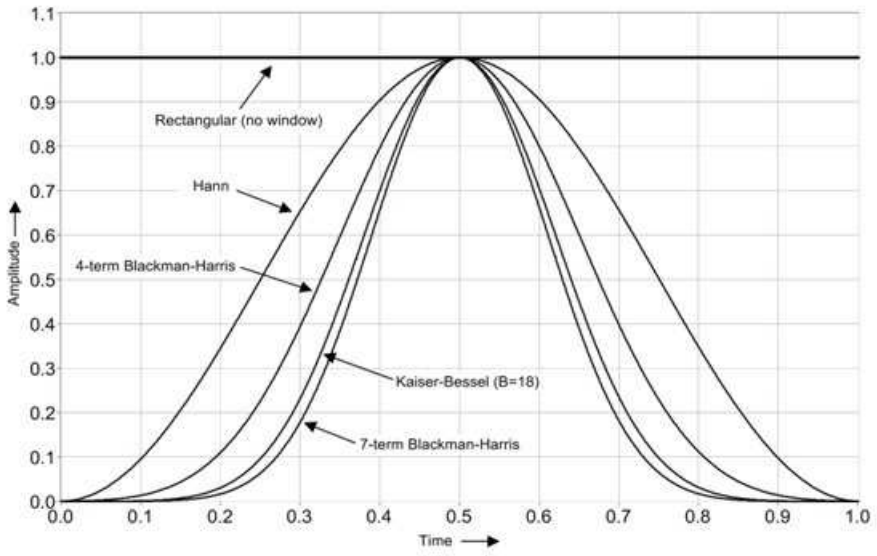

Figure 2.1: Common window functions[4]

2.4 Ground Penetrating Radar

GPR is essentially a near-range bistatic radar, where it is characterised by having a transmitter and a receiver antenna which is separated by a short distance apart. In such a system, electromagnetic signals are directed towards the target surface by the Tx antenna, where

the signals will partially reflect back towards the antenna, but more importantly, the main portion of the signal will penetrate the surface and is then scattered by any contrast in subsurface material. This scattered signal is then propagated back to the Rx antenna. There also exists a monostatic GPR arrangement where a single antenna is responsible for both transmitting and receiving, but in this project only the bistatic method will be investigated for antenna design[21].

2.5 GPR Antenna

"It is believed that the main breakthrough in GPR hardware can be achieved in the antenna design"[20]. Antennas are one of the most critical elements in a ground penetrating radar system. They should satisfy a number of requirement but the most important one is the wide frequency band. Due to the fact that GPR is essentially a near-range radar, its antenna elements should possess low coupling between the transmitter and receiver, both should also have short ringing effect.

As GPR antennas operate very close to the ground and sometimes in contact with it, the changes in ground properties, which includes the types of ground medium and its elevation, this should not strongly affect the antennas performance. Hence when obtaining a GPR antenna's characteristics one should not only measure them in free space but in a realistic ground penetrating environment[21].

2.6 Ultra Wide-Band (UWB)

Ultra wide-bandwidth is defined when the system has a an operating bandwidth f_b greater than 20% measured at the -10dB points, where narrow bandwidth is less than 1% at the -10dB point. A system is also considered UWB if the operating bandwidth is greater than 500MHz[5][16][17].

Figure 2.2 illustrate this:

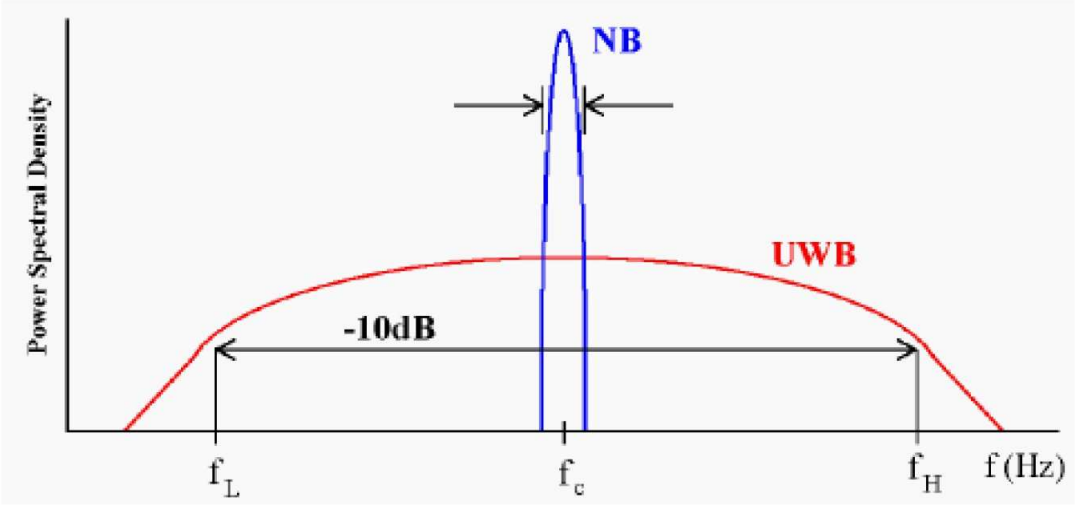

Figure 2.2: UWB definition[2]

Where $f_b = \frac{(f_h - f_l)}{f_c}$ and $f_c = \frac{f_h + f_l}{2}$ [2]

$f_h =$ Upper bandwidth frequency

$f_l =$ Lower bandwidth frequency

$f_c =$ Center frequency

2.7 Reflection Coefficient

The voltage reflection coefficient, Γ,is defined as:

$$\Gamma = \frac{Z_L - Z_o}{Z_L + Z_o}$$

The reflection coefficient is also equivalent to the scattering parameter S11, where Z_L is the load impedance and Z_o is the antenna characteristic impedance. The function of S11 will be elaborated in the next section where the VSWR is defined[5].

2.8 Voltage Standing Wave Ratio (VSWR)

The VSWR is a way of calculating how well two transmission lines are matched. The number for the VSWR ranges one to infinity, with one meaning that the two transmission lines are perfectly matched. With regards to antenna design, a VSWR that is as low as possible is desired because any reflections between the load and the antenna will reduce the effectiveness of the antenna. The VSWR is defined as:

$$VSWR = \frac{1+\Gamma}{1-\Gamma}$$

Where Γ is defined previously as the reflection coefficient[5].

2.9 Radiation Pattern

The radiation pattern indicates how directionally the antenna is radiating power, this is measured as the 3 dimensional far-field spread around the antenna. The radiation pattern required for GPR applications must be unidirectional, this means that power radiated must be more focused at a narrow angular direction rather than spread evenly around the antenna. The need for this characteristic is to eliminate ambiguous target detection. Figure 2.3 illustrates this.

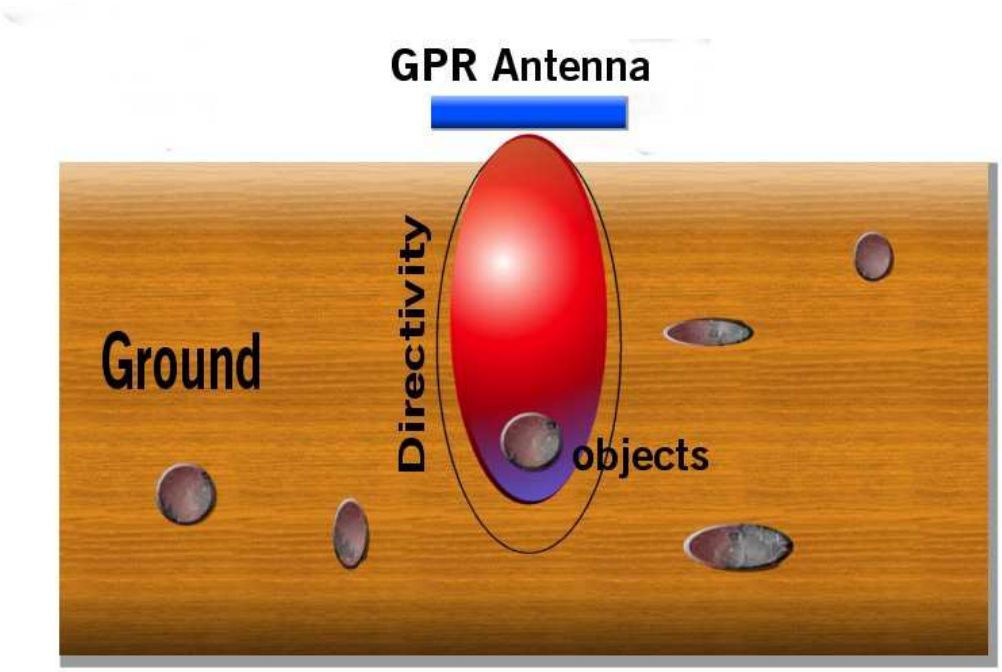

Figure 2.3: GPR directivity

2.10 Radiation Efficiency

The radiation efficiency η of an antenna is the ratio of the total power radiated by an antenna to the net power accepted by the antenna at its input terminals during the radiation process[22]. Where:

$$\eta = \frac{\mathbf{P_r}}{\mathbf{P_a}}$$

Where $P_r = \text{Total radiated power}$

$P_a = \text{Net power accepted}$

2.11 Antenna Gain

There are two different types of antenna gain, being the directive gain and the power gain. The directive gain is referred to as the directivity and the power gain simply as gain. The directivity is defined as the radiation intensity in a direction θ relative to the average intensity of an isotropic radiator. This can also be expressed in terms of the maximum radiated-power density at a far-field distance R relative to the average density if an isotropic radiator at R [23]:

$$G_d = \frac{\mathbf{P_{max}}}{\mathbf{P_t}/4\pi\mathbf{R^2}}$$

Where $P_{max} = \text{Maximum power radiated}$

and $P_t = \text{Total power radiated}$

The power gain or gain $G_p$of the antenna referred to an isotropic source is the ratio of its **maximum** radiation intensity to the intensity of a lossless isotropic source with equal power input[23]:

$$G_p = \frac{\mathbf{P_{max}}}{\mathbf{P_o}/4\pi\mathbf{R^2}}$$

Where $P_o = \text{Total power accepted}$

2.12 Termination Resistor

The purpose of a termination resistor is to minimise unwanted reflections on a transmission line and hence assuring maximum signal integrity. Applying this component to the edge of an aperture, it becomes an impedance termination resistor and increases the bandwidth of the antenna as low frequency reflections from the edges are absorbed. For a GPR application, the termination resistance also reduces the ringing effect from buried object. The effectiveness of the termination will depend on how closely the resistance value matches the feed point impedance of the antenna, but it has been shown that a slightly higher resistance value compared to the impedance gives an optimal effect. [10, 11, 12, 14]

2.13 Cross-Coupling

In a bistatic antenna configuration, cross-coupling is the signal travelled directly from the transmitter to the receiver. The level of cross-coupling and clutter must be minimised in a GPR antenna configuration as only the reflected signal from the buried object is desired[18]. This is illustrated in Figure 2.4.

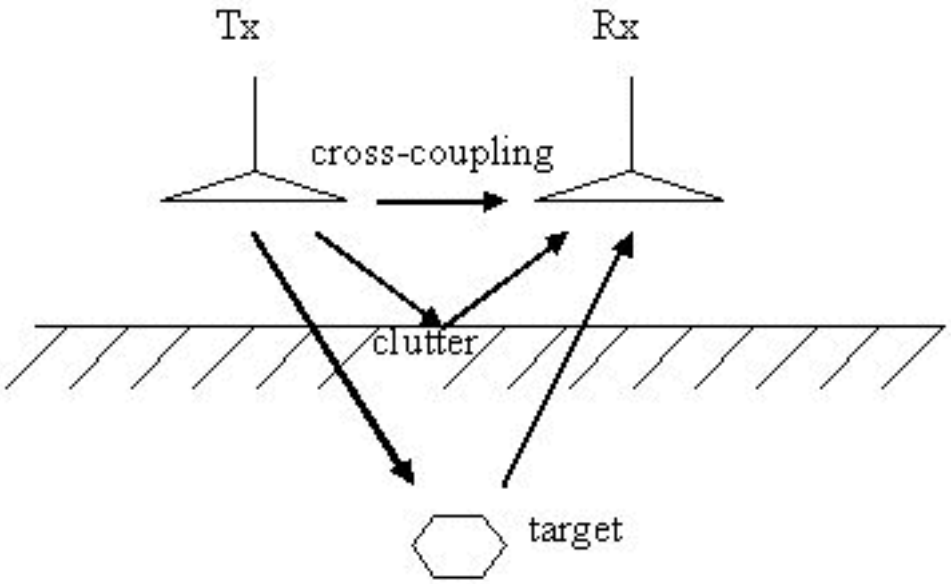

Figure 2.4: Illustration of cross-coupling and clutter of signals

2.14 Conclusion

This chapter discussed the relevant background technology used in this project. Method of moment (MoM) and finite difference time domain (FDTD) are two methods used to model the subsurface transit time response done in Chapter 3. Definitions of ground penetrating radar (GPR) and ultra wide-band (UWB) are discussed. Antenna properties mentioned in this chapter are all essential elements considered during the modelling and fabrication of the fat dipole GPR antenna designed in this project. The knowledge gained from the subsurface simulations done in the next chapter has familiarises me in simulating with FEKO, especially with the planar multilayer green's function which was extensively used in antenna modelling.

Chapter 3

Ground Penetration Transmitter-Receiver Time Response Simulations

The applications of ground penetrating radar has being hugely increased to gain valuable information such as water content of soil, depth of water, buried objects and void detection [7]. In this chapter, a study conducted by K.P. Mudhopadhyay(2004) investigating the EM waves propagating through layered media simulated using FDTD method will be shown, and compared to results obtained using FEKO, a frequency based MoM code.

3.1 Simulation Configuration

Figure 3.1 displays how the simulations are setup in FEKO. The receiver antennas are placed 2, 4 or 5.25 metres apart from the transmitter antenna. These $\lambda/2$ dipole antennas are situated in the sand layer between the clay layers. Above and below the clay layers are perfect conducting boundaries. The length of these antennas has been calculated with regards to the speed of propagation calculated with sand's relative permittivity ($\epsilon_r = 20$). The mid-layer has a thickness of 4 metres with the two clay boundaries each being 0.2 metres thick. The FDTD simulation is configured in the same manner where the only difference is that point source transmitter and receivers are used instead of antennas. The electrical property of the materials are shown in Table 3.1 [7].

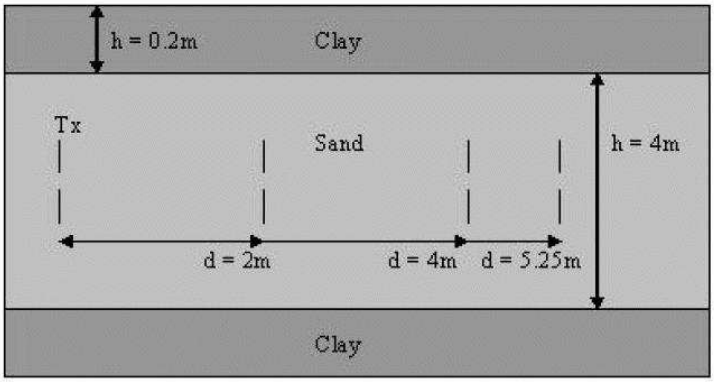

Figure 3.1: Dimensions of the layered media under investigation.

Table 3.1: Electrical properties of sand and clay used in computation.

Electrical Property	Sand	Clay
Electrical conductivity, σ [S/m]	0.0001	0.5
Relative dielectric permittivity, ϵ_r	20	40
Relative magnetic permeability. μ_r	1	1

FEKO's planar multilayer Green's function was used to define the layered media regions, where the influences of these dielectric regions are implicitly taken into account. This function uses less resource than modelling them as separate dielectric bodies. Figure 3.2 shows that this function can simulate the required subsurface conditions entirely with only the depth of media be taken into consideration. The width of the dielectric regions is undefined as surface equivalence principles is not implemented in this series of simulations[6].

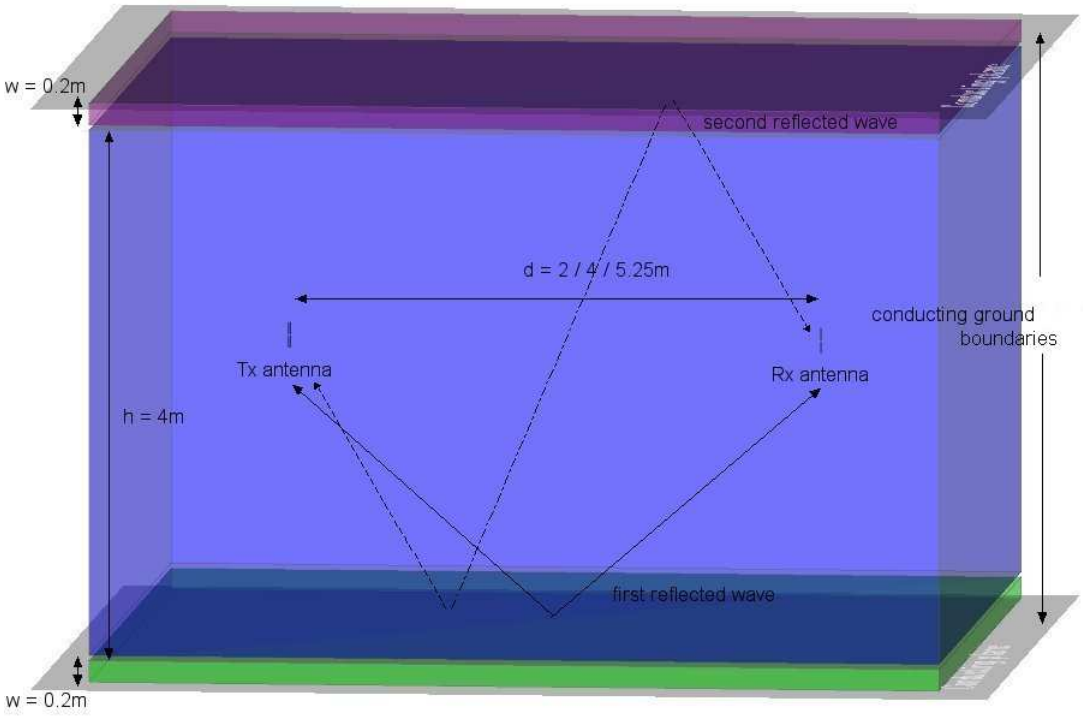

Figure 3.2: Subsurface simulation 3D model in FEKO

3.2 Excitation

In both simulations, the transmitter is excited with the same differential Gaussian pulse shown in Figure 3.3. The normalised power pulse has a time-shift $t = 10$ns and a 3dB pulse width $\tau = 3.33$ns with a nominal frequency of 100MHz. As FEKO is a frequency domain based software, one has to define the frequency intervals carefully to reduce the effect of aliasing in the time-domain. This requires the maximum simulating frequency to be large enough so that the whole spectrum of the exciting pulse is covered. For the Gaussian pulse used in the simulation, the maximum frequency f_{max} should be large enough such that the entire spectrum of the exciting pulse is covered, hence f_{max} was chosen to be approximately equal to four times the value of f_{3dB}, and the number of frequency points *N* is chosen so that total duration in the time-domain be long enough for all received and reflected pulse to have decayed, with this in mind, the frequency elements of the subsurface simulations were set to be $f_{max} = 225$MHz and $N = 46$[6].

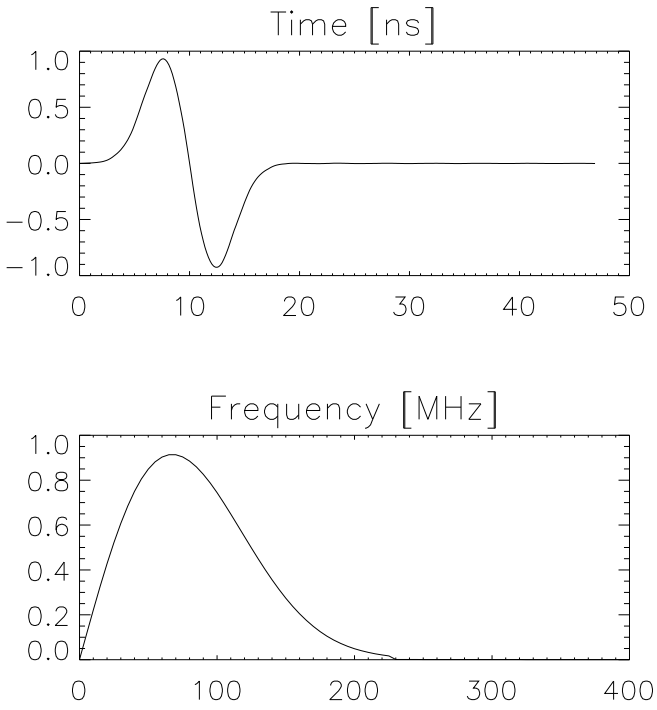

Figure 3.3: Transmitted pulse and its spectral representation.

3.3 Results

The transit time-response simulated with both methods corresponds to the calculated results. This is shown in Table 3.2, where response time t is calculated by the equation below:

$$\mathbf{t} = \frac{\mathbf{distance}}{\mathbf{velocity}}$$

$$= \frac{d}{c_0} \times \sqrt{\epsilon_r}$$

$$\epsilon_r = \text{Relative dielectric permittivity}$$

Figure 3.4 and 3.5 shows the results from FEKO and FDTD simulations. The two sets of results shown displays the difference in received signal time response as the distance between the transmitter and receiver increases. There are three separate waves visible in each of the plot. The first wave on each axis is the direct wave. It is the wave that travels directly from the transmitter to the receiver. The second wave on the axis is the first reflected wave, which is the superposition of the reflected wave from the top and bottom of the clay layer. The last wave on each axis is the second reflected wave, they

Table 3.2: Calculated time response

Antenna's Distance Apart	Antenna's Distance Apart	Receiver at 4m apart	Receiver at 4m apart
Direct *d* (m)	2	4	5.25
Direct t (*n*s)	**29.8**	**59.6**	**78.2**
1^{st}reflection *d* (m)	4.47	5.66	6.6
1^{st}reflection t (*n*s)	**66.6**	**84.3**	**98.3**
2^{nd}Reflection *d* (m)	8.25	8.94	9.57
2^{nd}reflection t (*n*s)	**122.9**	**133.2**	**142.6**

are the superposition of waves that reflected from both "top to bottom" and "bottom to top" clay layers before reaching the receiver. As can be seen in Figure 3.3, the transmitted waveform has been deformed by the lossy media. The radiation losses contribute towards the decrease in signal amplitude with increasing distance [7, 9]. There are three plots obtained from computations done by FEKO and FDTD, simulating the transit distance respectively of 2, 4 and 5.25 metres. These results show a distinct direct and reflection time response difference between each transit distance.

The combination of the two sets of results (Figure 3.6) shows that MoM and FDTD simulations correspond well with each other, with receiver signals appearing at the same response time. FEKO's results clearly display a difference in shape of the receiver waveform from FDTD, this inverse in receiver signal polarity compared to the FDTD point source (Blackman-Harris window function) response is caused by the signals been differentiated by the dipoles, where the $1/4$ wavelength (operating frequency of 100MHz) of the dipole arms are multiplied by $\sqrt{\epsilon_r}$ to simulate accurate dipole appertures within the sand medium. As dipole antennas are resonating elements, any pulse fed to it will cause a ringing effect, hence the longer pulse duration. [13]

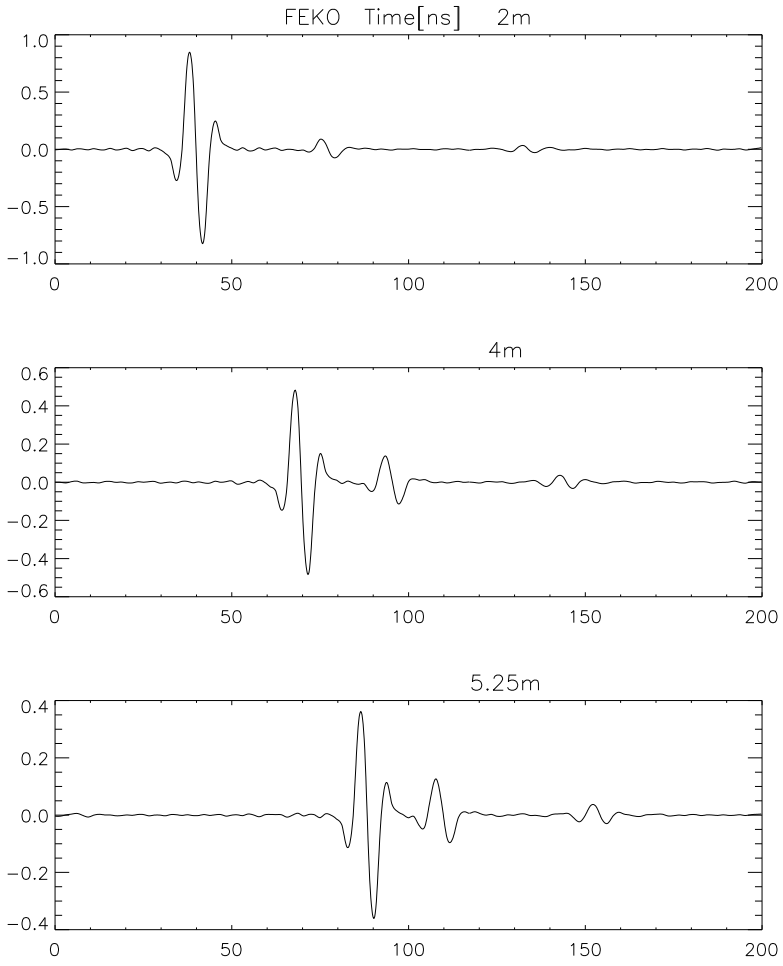

Figure 3.4: Received waveforms obtained using FEKO.

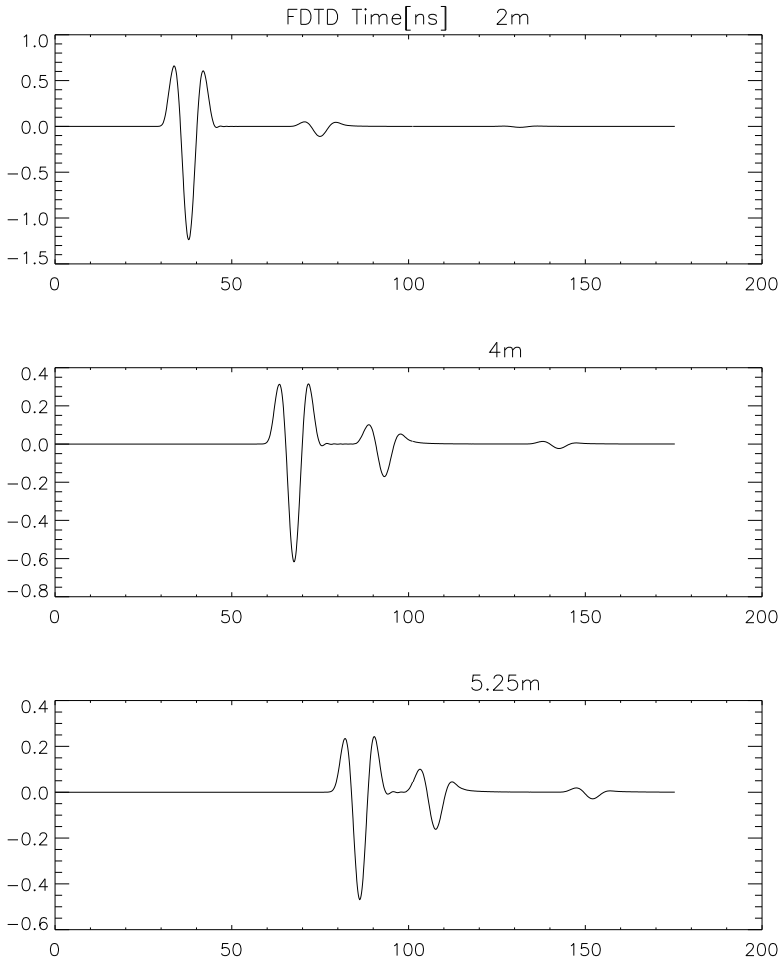

Figure 3.5: Received waveforms obtained by K.P. Mukhopadhyay using FDTD.[7]

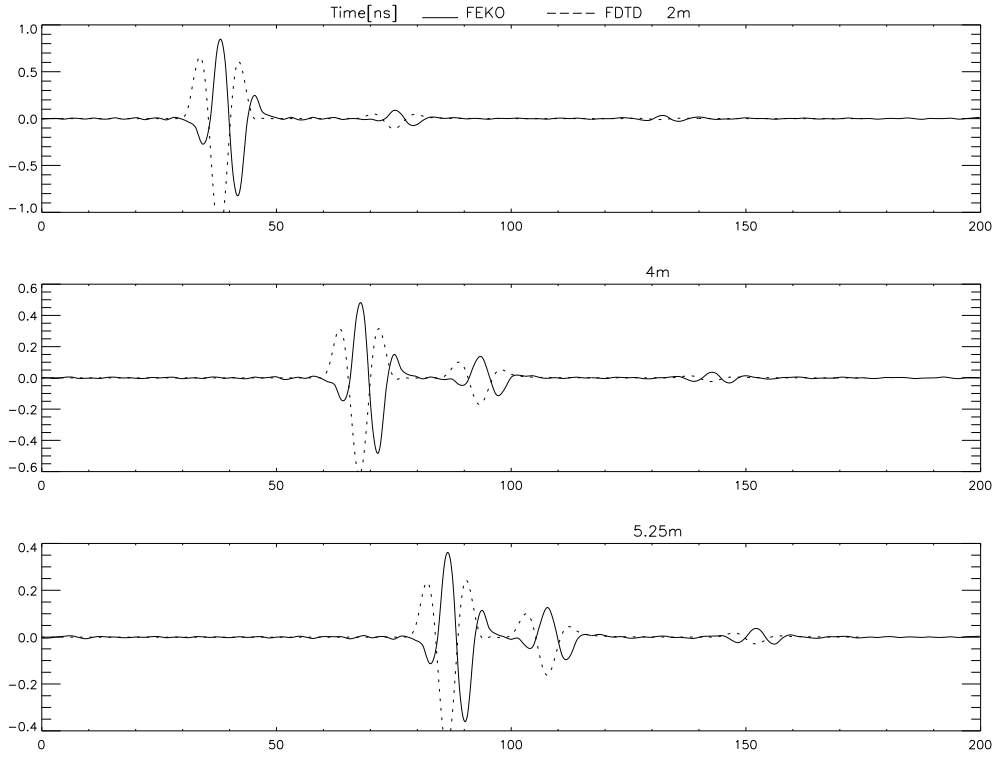

Figure 3.6: Over-plot of FEKO and FDTD receiver waveforms.

3.4 Conclusion

In this chapter, FEKO was used to compare results of transit time response obtained from a finite difference time domain (FDTD) method simulator. A transmitter and receiver antenna are positioned a set of distances apart situated in a subsurface layered media (sand and clay), time response of the direct and reflected EM waves propagating through the media. As shown in Figure 3.6, FEKO's simulation results shows that the MoM planar multilayer Green's function's ability to compute transit time in subsurface layered media has a comparable accuracy to one using FDTD method. Although results from FDTD (Blackman-Harris function point source) simulations seems less clutter, implementation of dipole antennas gives a much more realistic result when comparing shapes and duration of waveforms. If only the direct and reflected wave's time response is needed, then FDTD point source simulation have proven to have a much clearer time response indication. Further studies can be conducted on the shape change of receiver waveforms, this will provide a better understanding of subsurface media properties.

Chapter 4

Fat Dipole Modelling

Antennas are one of the most critical elements in a ground penetrating radar system. For this project they should satisfy a number of requirements including ultra wide frequency bandwidth, low cross-coupling, short ringing effect and an unidirectional radiation pattern. As GPR antennas operate very close to the ground and sometimes in contact with it, it should be designed and constructed mechanically strong and yet mobile. Due to these reasons, when obtaining a GPR antenna's characteristics, it is required that to not only measure them in free space but in a realistic ground penetrating environment. [20][21]

The fat dipole antenna is chosen to be investigated and modelled due to its simplicity in design and UWB nature. Later on in this section, modification will be implemented to the fat dipole design to improve its performance.

4.1 Modelling of UWB Fat Dipole Antenna

The UWB fat dipole in Figure 4.1 designed by the Korea Electro-technology Research Institute (KERI) and Microline Co. Ltd. has been chosen to be investigated and modelled for our GPR system due to its simplicity in design and its bandwidth performance. The design has proven to have VSWR capability of below 2 at the bandwidth from 80MHz to 310MHz shown in Figure 4.2. This section shows the results simulated by FEKO compared to ones obtained by KERI and Microline.

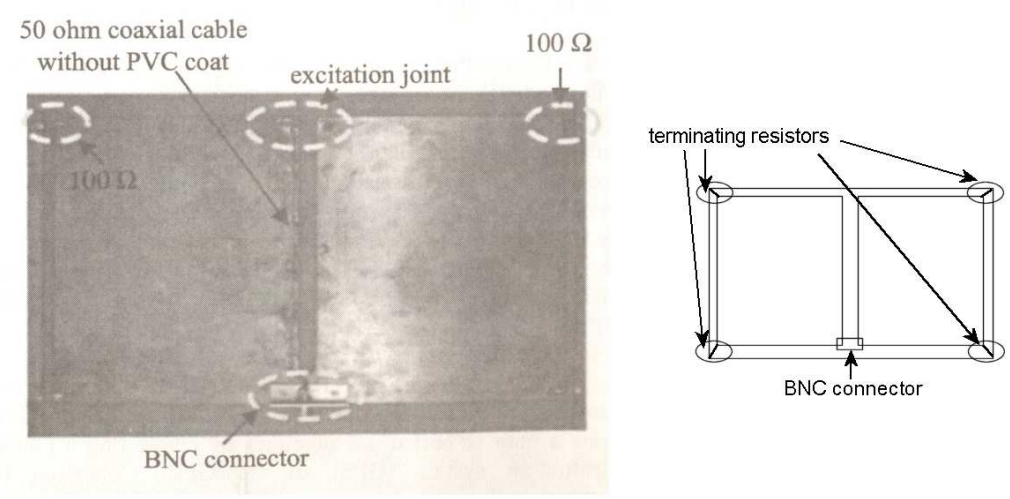

Figure 4.1: Picture of KERI and Microline fat dipole[14]

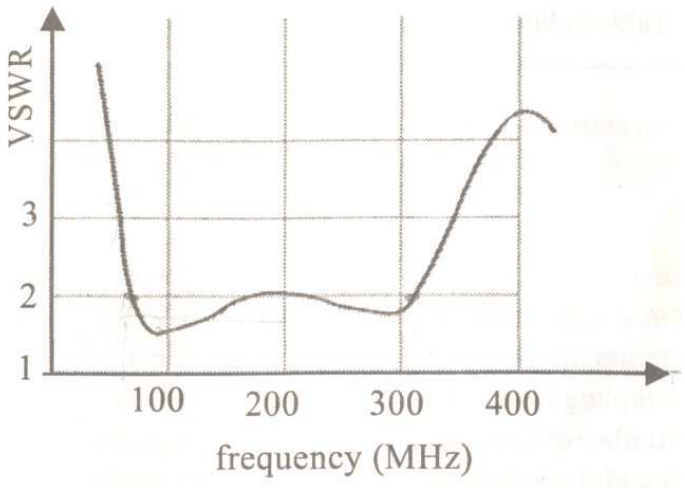

Figure 4.2: 100 - 400MHz fat dipole VSWR[14]

The fat dipole from Figure 4.1 was modelled in FEKO shown below. This was done by implementing the planar multilayer substrate function that incorporates Green's function to solve microstrip EM problems. The antenna dimensions includes dipole arms each 240mm x 500mm with 50mm gap between them, FR 4 ($\epsilon_r = 4.8$) substrate, width of 1mm, and a grounding parabolic reflector used in KERI and Microline's experiment. Figure 4.6 is a FEKO graphical representation of the antenna:

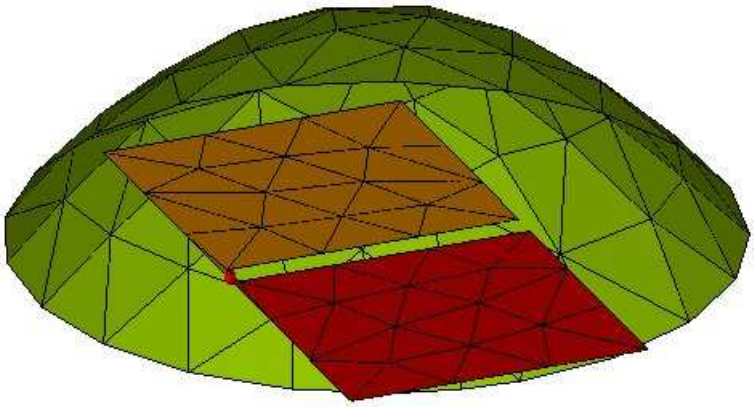

Figure 4.3: KERI and Microline fat dipole in FEKO

When feeding the excitation to a fat dipole antenna in FEKO, either a wire feed segment or an edge feed can be used. The structure of the feed model has to be modified to achieve either excitation. Although the wire feed worked well for our model, implementing the edge feed has shown an improvement over the wire feed. The feed structures are shown in Figure 4.4 and 4.5:

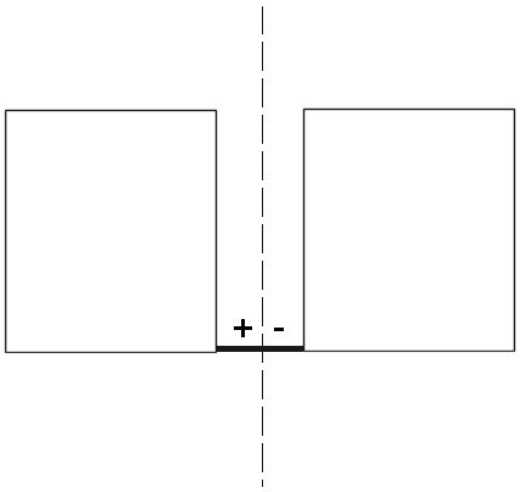

Figure 4.4: Fat dipole model with wired feed segment structure

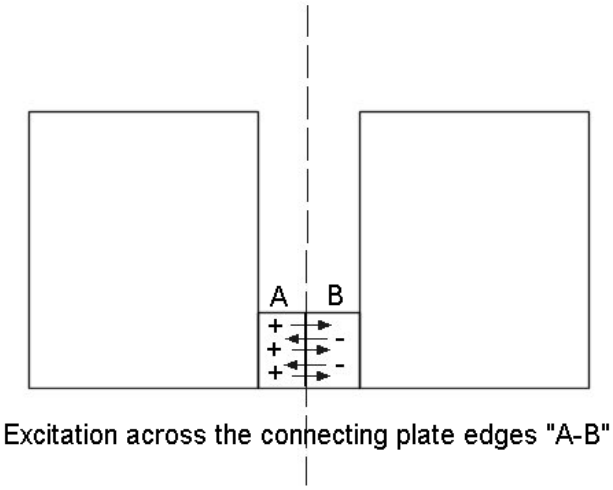

Figure 4.5: Fat dipole model with edge feed structure

The results of the simulation is shown in Figure 4.6. The UWB quality shown matches the result in Figure 4.2 obtained by KERI and Microline, with VSWR and return loss displayed is agrees with the physical test figures (VSWR under 2 for the investigating bandwidth), where the operating band showed less then 30MHz difference. This result establishes planar multilayer planar Green's function's ability to simulate this antenna architecture.

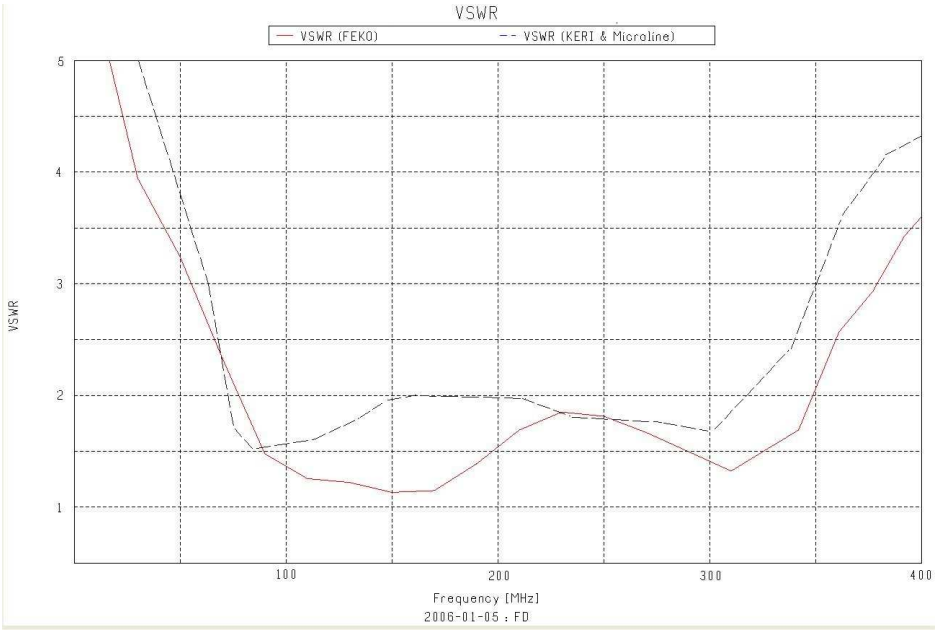

Figure 4.6: KERI and Microline fat dipole VSWR using FEKO

The above results prove the feasibility to continue modelling with this antenna design. In

the next section, adaptation of this design using a planar reflector for the 400-800MHz region is attempted.

4.2 Modelling of 400 - 800MHz Fat Dipole

There are several modifications that have been implemented to fulfil this project's specific antenna requirements. In this case, the most important alteration is the change in physical size of the radiating dipole arm to compensate for our specific operating bandwidth. A polystyrene foam substrate was used instead of the FR-4 PCB substrate. This method has proven to be highly effective for GPR applications as it allows the ground plate to direct more energy back into the ground, increasing the efficiency of the antenna[14]. The antenna is also modelled 10mm above the ground due to variable ground surface in a real GPR application. The ground's electrical properties are set to the value of compact sand, reason being this material is available for result validation at a later stage. Table 4.1 shows the substrates and ground properties.

Table 4.1: Dielectric Properties

Substrate	FR-4	Polystyrene	Ground (Sand)
Relative permittivity ϵ_r	4.8	1.08	10
Electrical conductivity, σ [S/m]	$1e^{-8}$	$5e^{-14}$	$1e^{-5}$

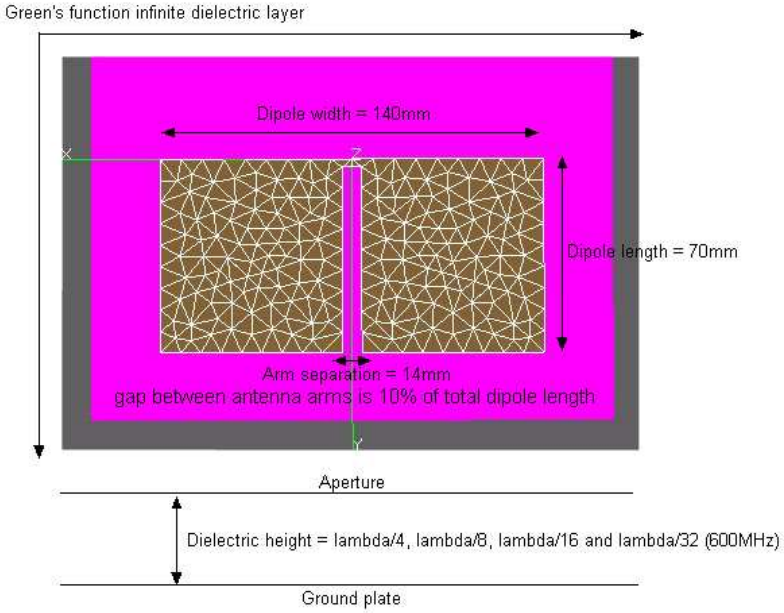

Figure 4.7: FEKO model of 400 - 800MHz fat dipole

To design the best fit antenna possible, several substrate heights have been modelled to investigate how it affect the operating bandwidth and centre frequency of the antenna, a graphical representation of this antenna is shown in Figure 4.7. The heights that are chosen are $\lambda/4$,$\lambda/8$,$\lambda/16$ and $\lambda/32$ with the centre frequency being 600MHz. The reflection coefficient of the antennas are shown in Figure 4.8.

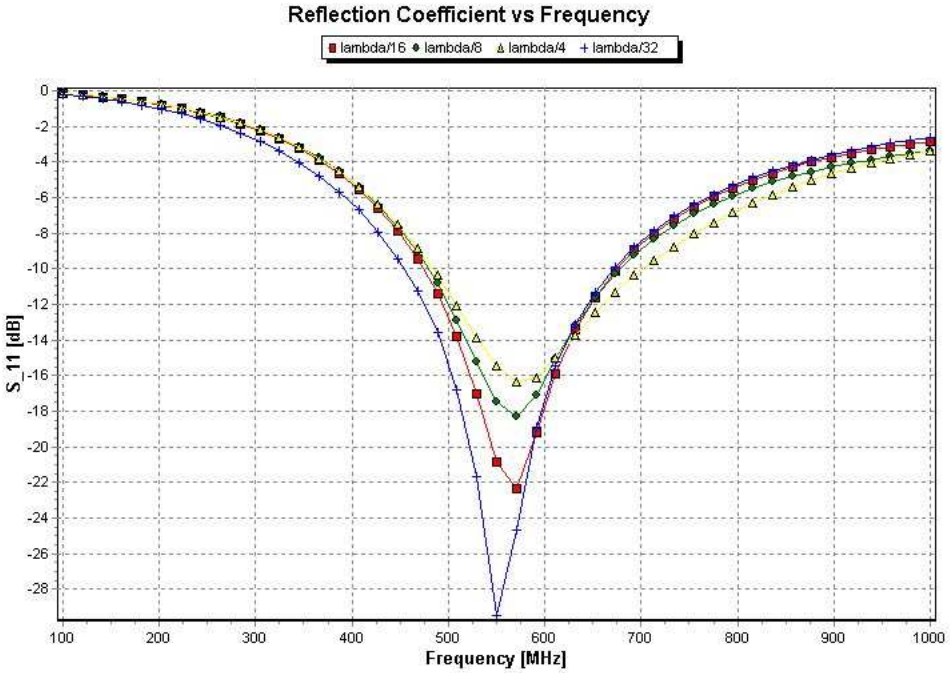

Figure 4.8: S11 of various fat dipole substrate heights

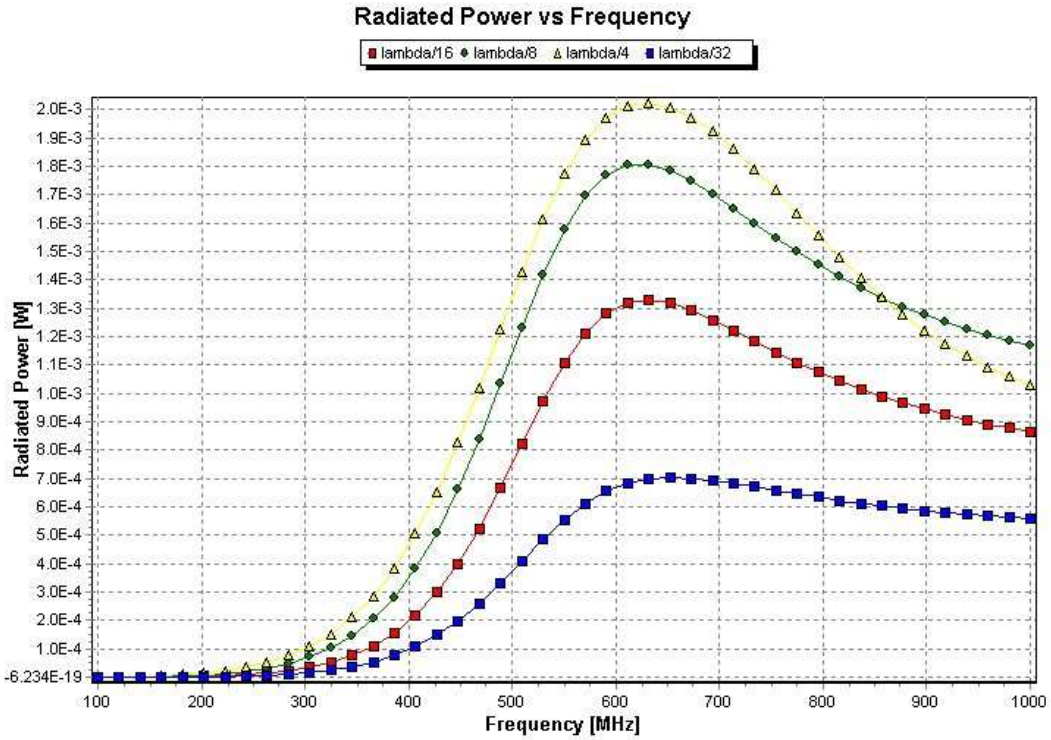

Figure 4.9: Power radiated

From the reflection coefficient of the five models shown in Figure 4.9, we can see that the values of both the 10dB bandwidth and the centre frequency S11 increases with

decreasing substrate height, but can also be observed that radiated power decreases with increasing height, where radiated power is obtained by using the excitation source data function in FEKO, which calculate the radiated power from the input power less the returned power at the feed point. Both of these properties are important when designing an antenna. Although having a high radiated power is desired, it is crucial that it is radiated in the correct direction, and in this case it must radiate mostly towards the ground. Figure 4.10 are the near field results along the z-axis which is the vertical axis perpendicular to both the antenna and the ground surface. This indicates the amount of power radiating into the ground, where z = 10mm is the point of contact with the ground. From this we can see that the$\lambda/8$ model proves to have the most power radiating into the desired direction and was chosen for further development. The vertical radiation pattern displayed in the Figure 4.11 shows that this dipole design has the directivity needed for GPR applications.

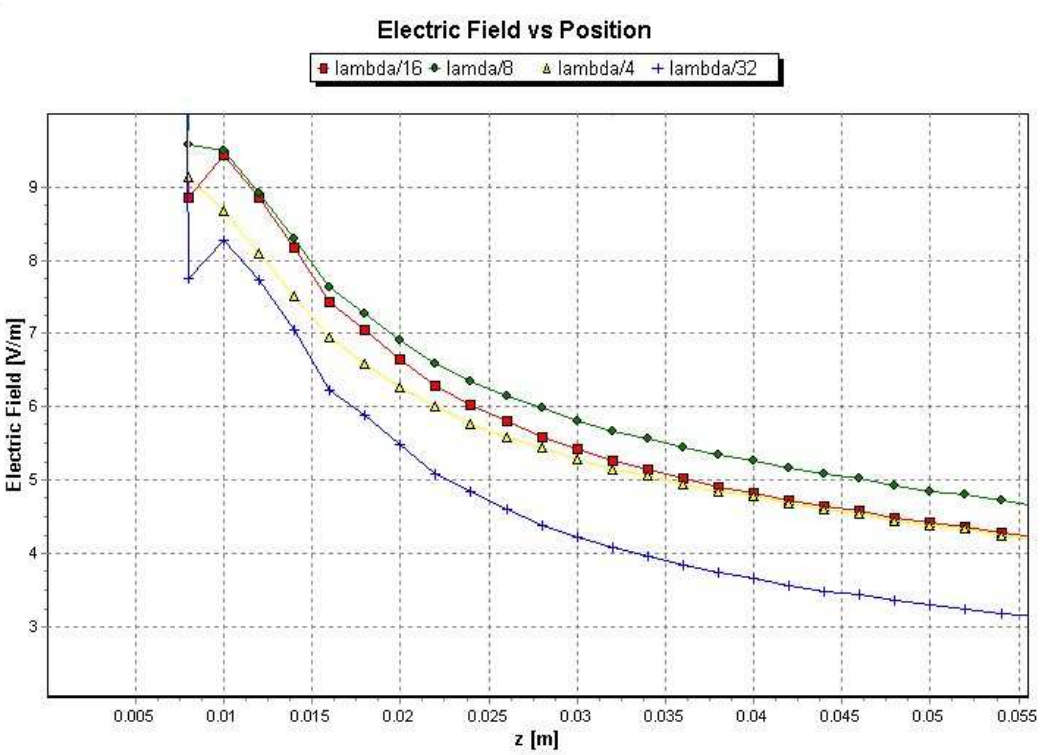

Figure 4.10: Electric near field indicating amount of power radiating vertically into the ground

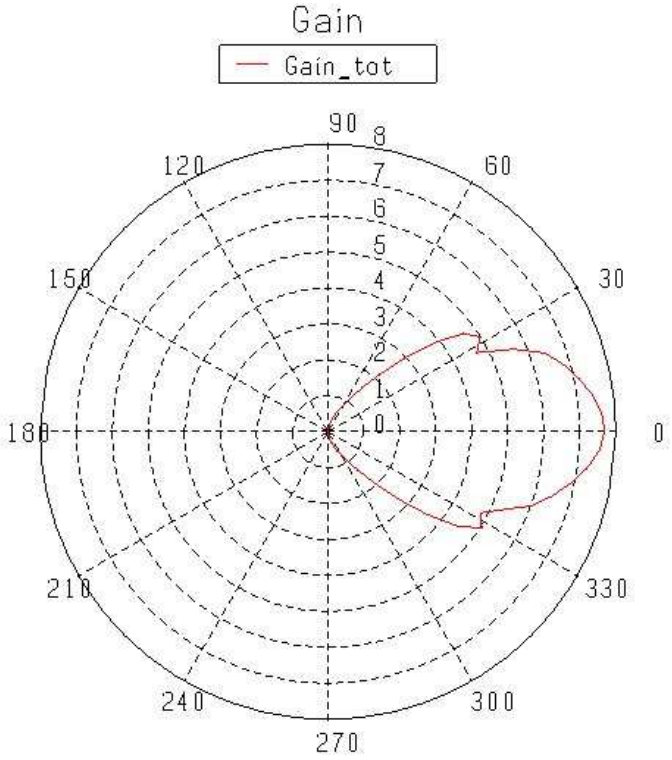

Figure 4.11: Fat dipole radiation pattern at 600MHz

4.3 Modelling of Cased Fat Dipole with Edge Terminating Resistors

The current antenna design can be improved by constructing metallic barriers around the polystyrene dielectric. This will direct more energy back into the forward direction and also reduces the cross-coupling between the antennas. This structure also allows the possibility of connecting the edge terminating resistors to the grounding metallic box. Due to ground surface changes, it is also unlikely to have a fixed air gap with the ground at all times, hence a 10mm thick Teflon plate is implemented to replace the air gap. This provides a layer of protection against abrasions that may occur to the aperture by the ground terrain during GPR operation. This dielectric shielding of an antenna in a medium has shown in previous studies observed by Stellenbosch University's antenna research group that the aperture dimensions can be reduced for the same operating frequency, however with the trade-off of bandwidth and efficiency, depending on the thickness of the dielectric[11]. The dimensions of the cased fat dipole consist of the two dipole arms being 133x140mm separated 14mm apart (approximately 10% of arm length) situated on top of a polystyrene foam block of 280x140x62.5($\lambda/8$ of 600MHz)mm, surrounding cavity of 280x140mm having a height of 52.5mm creating 10mm spacing between dipole arms and

cavity for terminating resistor placements. Figure 4.12 - 4.14 and Table 4.2 indicates the physical dimensions of the antenna.

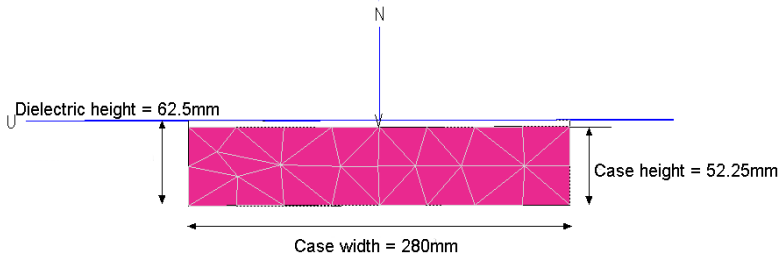

Figure 4.12: Front view of the simulated antenna model

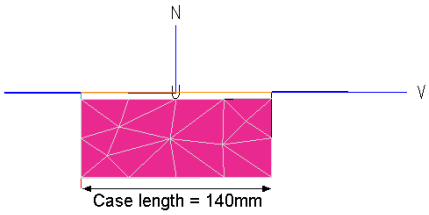

Figure 4.13: Side view of the simulated antenna model

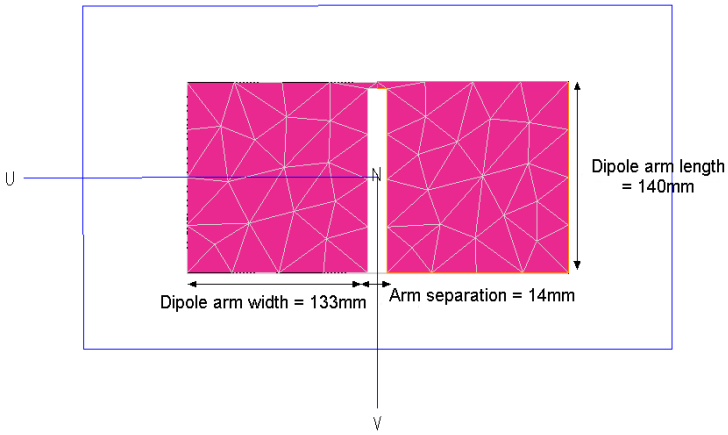

Figure 4.14: Top view of the simulated antenna model

Table 4.2: Cased fat dipole Antenna simulation dimension in mm

Antenna Elements (mm)	Width	Length	Height
Cavity	280	140	52.5
Aperture (per dipole arm)	133	140	0.5
Teflon Layer	280	140	10
Polystyrene Foam Dielectric	280	140	62.5 ($\lambda/8$)

Before modelling the antennas with terminating resistors, the impedance of the antenna will have to be determined. As mentioned in Chapter 2, the terminating resistors are best chosen to be of a higher value than the feed point impedance of the antenna. As shown in Figure 4.15, the magnitude of the feed impedance can be observed to be an average of 210Ω across the operating band, hence 250Ω terminating resistors were used to simulate the antenna return loss. The terminating resistors are placed in the four edges of the box connecting to the outer two edges of each arms of the dipole. Due to the plane of electrical symmetry, these resistors will not influence the electrical fields within the antenna. Figure 4.16 illustrates the resistor connections.

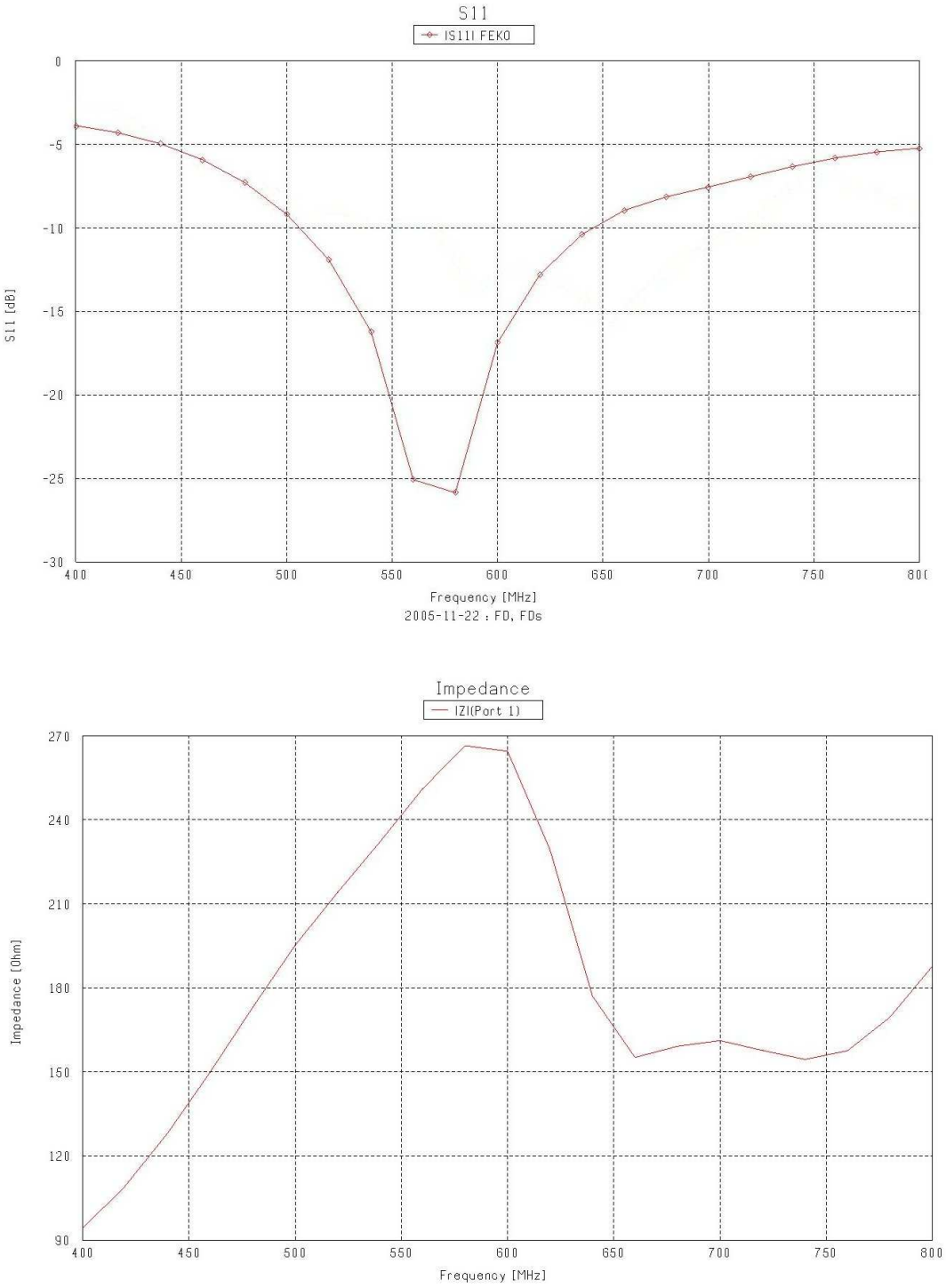

Figure 4.15: Impedance and S11 simulated result before implementing terminating resistors

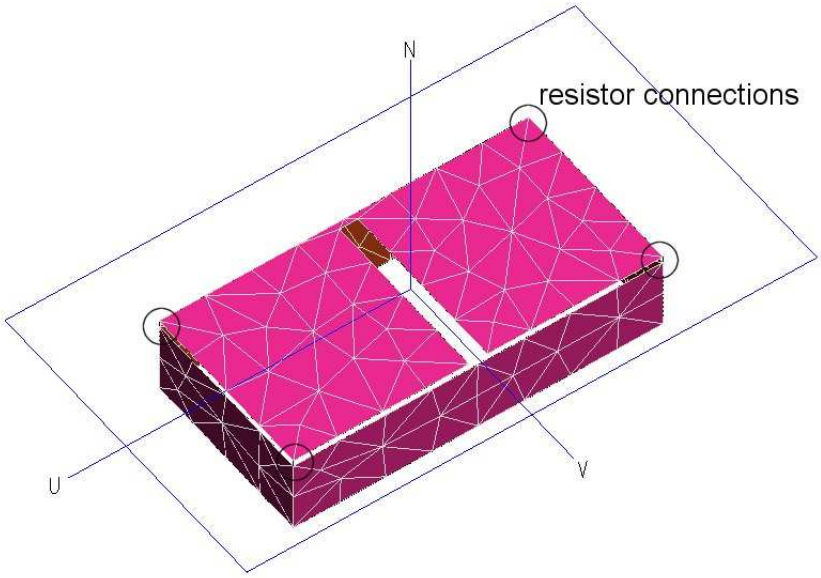

Figure 4.16: Edge termination resistor connections

The improvement in antenna performance can be observed in Figure 4.17, illustrating the effects of terminating resistors absorbing the low frequency reflections, hence increasing the operating band of the fat dipole. The simulated electric near field displayed in Figure 4.17 shown an improvement in efficiency compared to the result shown in Figure 4.10, where by the casing of the dielectric has achieved maximising the transmission of energy into the ground.

At the centre frequency of 660MHz, the 3D radiation pattern showed the desired unidirectional, half hemisphere radiation pattern in the direction of the ground having approximately 10dB gain.

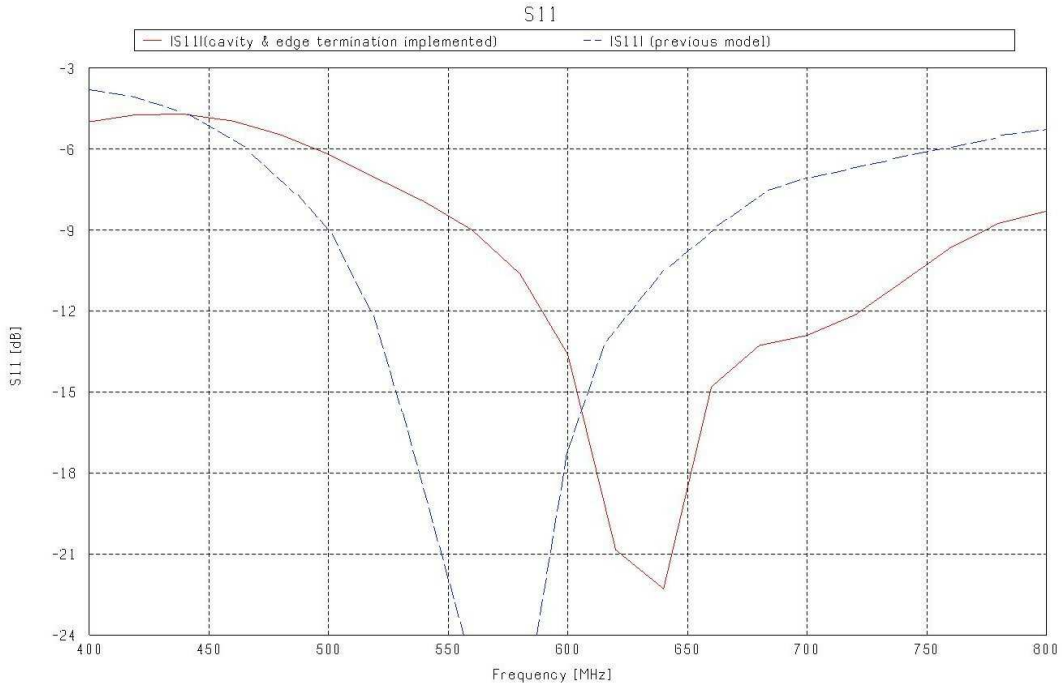

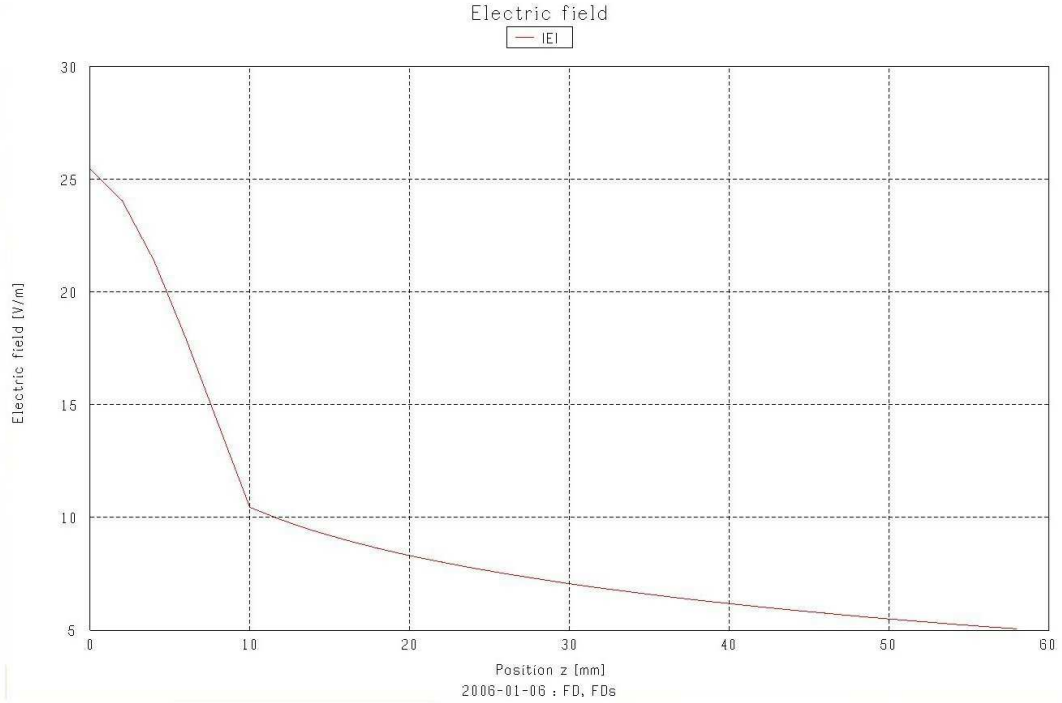

Figure 4.17: Improved S11 and near field result (at 600MHz) after implementing termination resistors

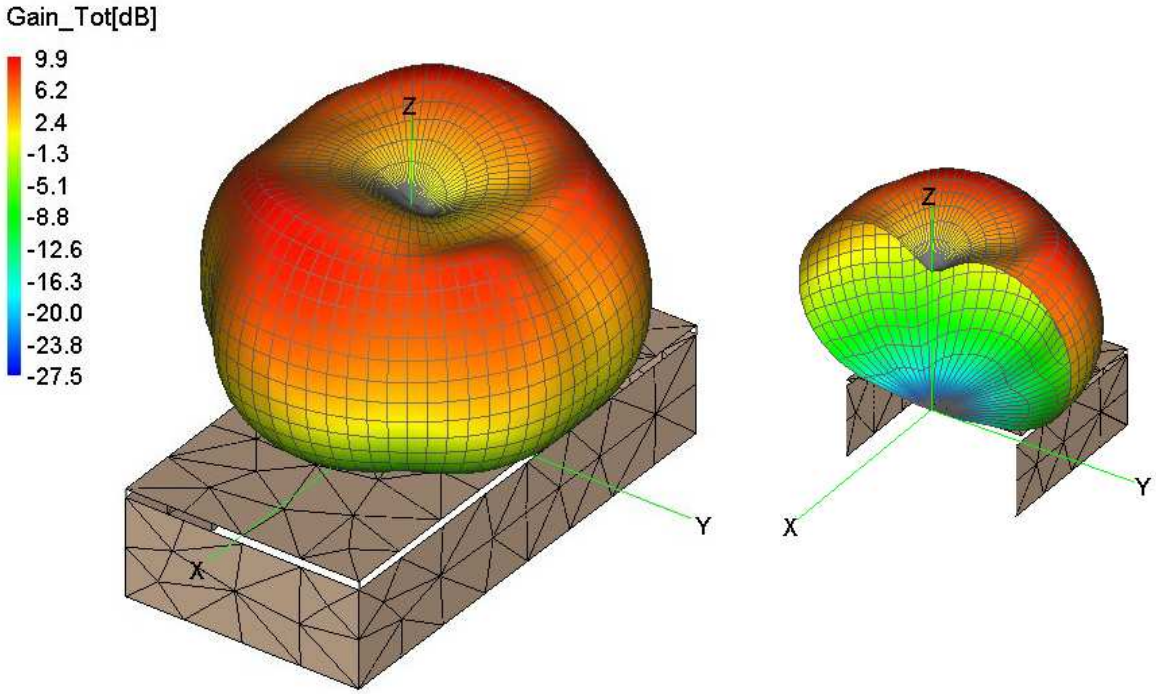

Figure 4.18: 3D radiation gain pattern indication the directivity of the cased fat dipole

The radiation efficiency, which is obtained by using the efficiency source data funtion contained within the FEKO post processing program, is calculated as the percentage of total power radiated over the antenna input power at a specific frequency, is also an important parameter to consider in an antenna design. The result obtained by the final antenna model shown in Figure 4.19 displayed a 50% efficiency from 500 MHz onward, proving this design's improvement over the traditional absorptive GPR antenna which achieves its half hemisphere radiation pattern by absorbing the power that radiate backwards, hence losing half of its radiation efficiency. The results also show that the antenna radiates poorly below 450MHz, this is due to the lower frequency energies absorbed by the termination resistors.

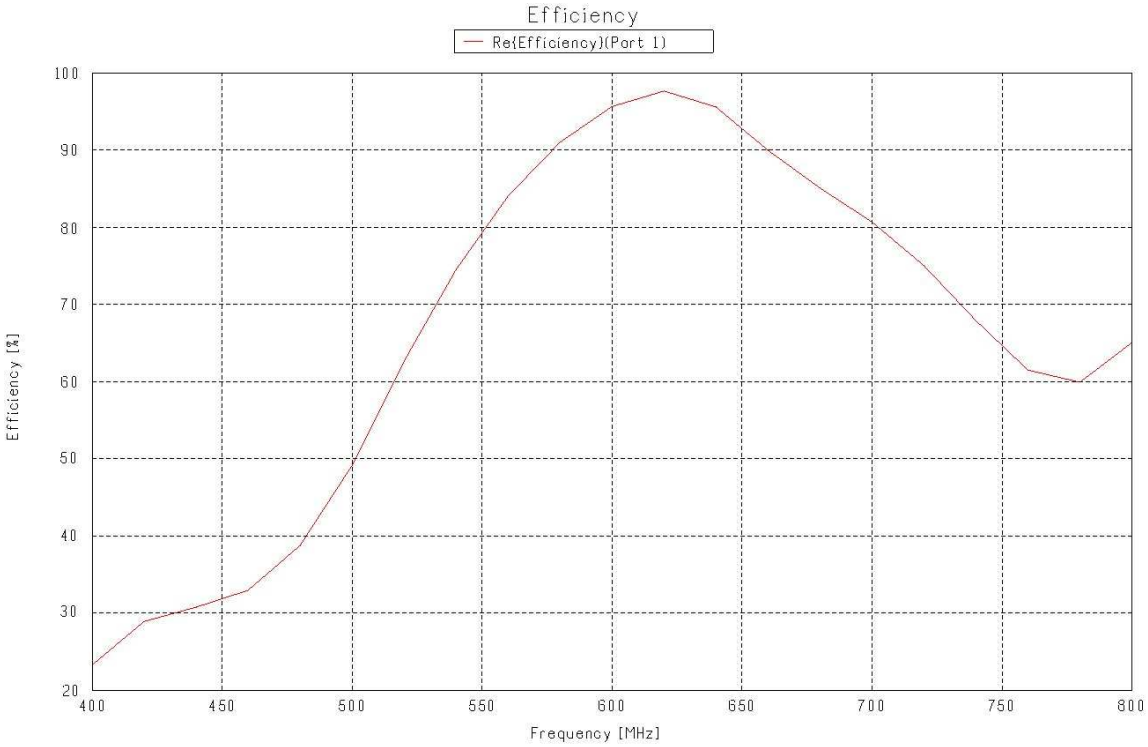

Figure 4.19: Radiation efficiency of the final antenna model

4.4 Conclusion

In Chapter 4, a 100-400MHz UWB fat dipole antenna designed by Korea Electro-technology Research Institute (KERI) and Microline Co. Ltd. was reviewed. This design implements the wide-band characteristics of an extended width patch dipole for GPR applications. FEKO was used to model this antenna design and compare the simulated results with the original developer's VSWR. The results shown in Figure 4.6 validate the feasibility of modelling such design in FEKO for this project.

After validation of the fat dipole design, several 400-800MHz dipoles were simulated with different dielectric (polystyrene foam) and substrate height to investigate how its effect the bandwidth, radiated power, electric near field and radiation pattern. This was done to find the best suited antenna for fabrication and testing. Out of the$\lambda/4$,$\lambda/8$,$\lambda/16$ and $\lambda/32$ substrate heights, it was determined that $\lambda/8$ is the best fit with regards to our antenna requirement, which is having the maximum radiated power that is directed into the ground.

With the GPR specifications in mind, an improved model was created using a Teflon dielectric layer on the bottom of the aperture to protect the antenna from the ground (real ground may have rough surfaces, hence a strong non-conductive material is needed for

protection against abrasion against the aperture). A cavity type design is also implemented to maximise the energy directed into the ground, this design is validated with the simulation results show in Figure 4.18 and 4.19. This design also provides conductive ground for connecting edge terminating resistance to the aperture, where it has proven that it has increased the operating bandwidth by reducing lower frequency reflections shown in Figure 4.17. The next stage of this project is fabricating the modelled antenna and verifying its performance.

Chapter 5

Antenna Construction and Verification

Through investigations done in the previous chapter, the cased fat dipole model showed desired GPR antenna performance needed for this project. In this chapter, the method of construction and return loss verification with the Agilent E5062A network analyser are shown.

5.1 Antenna Aperture and Casing Construction

The antenna elements are constructed using 0.5mm tin plate due to it being the easiest material to solder feed onto. The casing of the antenna is constructed using 1mm thick aluminium plate, pop riveted to form a robust open ended box. The polystyrene dielectric foam is then placed within the casing, with the dipole arms flush on top of the dielectric. This configuration allows a 10mm gap between the aperture and the aluminium casing for connection of terminating resistors.

5.2 Balun Feed

A dipole antenna needs to have a balanced feed: this means equal current must feed into each arms. A co-axial feed gives a positive source with reference to ground, hence it is impossible to feed the two dipole arms directly. To solve this problem one would require implementing a balun between the co-axial feed and the antenna. For this project, an RF transformer is a suitable balun, as its provides impedance transformation between the 50Ω co-axial cable and the input impedance of the antenna, at the same instance creating a balanced to the dipole arms. For this antenna design, the transformer is required to feed a 50Ω co-axial to a 210Ω impedance antenna. This is illustrated in Figure 5.1.

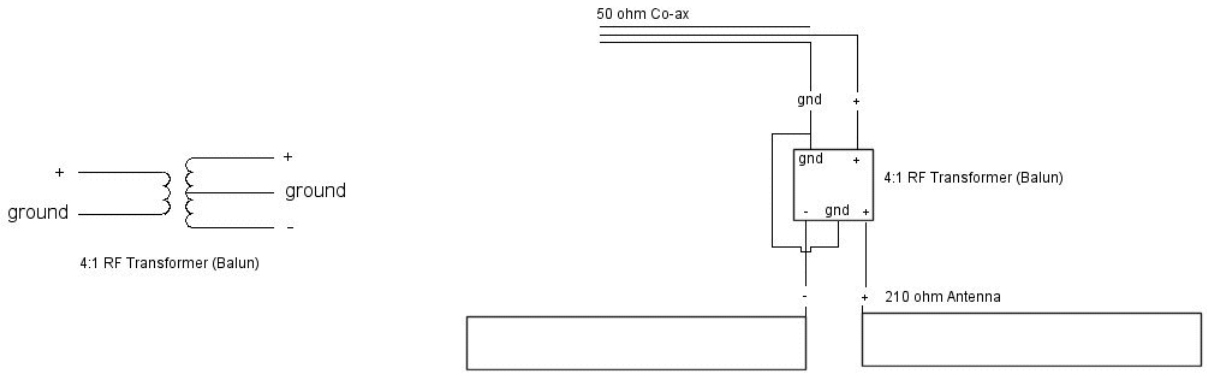

Figure 5.1: Balun architecture and antenna feed structure

A 4:1 transformer (TC4-1W shown in Figure 5.2) from mini-circuit was used for this design, as its has a correct winding ratio as well as a desired operating band of up to 800MHz. It is also relatively small in dimension making it possible to mount onto the antenna casing. A layout of how the balun is connected to the co-axial cable and the antenna is illustrated in Figure 5.1. The wires connected to each of the balun leads and dipole arms are kept less than $\frac{1}{10}$ of the minimum operating wavelength with equal dimension, this is to ensure minimal impedance mismatch and transmission line losses.

Figure 5.2: Picture of TC4-1W RF Transformer[Appendix B]

5.3 Terminating Resistors

Although the simulations were conducted using 250Ω termination resistors, due to availability, 271Ω resistors were used instead. These resistors are chosen to be chip resistors for

their performance at higher frequencies. To ensure robust resistor connection between the aperture and the aluminium cavity, small lugs were used to rivet the one end of the resistor to the grounding wall, and the other soldered onto the outer corners of the aperture. Due to chip resistors weak mechanical strength and connectivity, they were encased with insulation adhesives after leads were soldered onto both ends.

5.4 Return Loss Measurement

The reflection coefficient of the antenna was measured with the Agilent E5062A network analyser. The photograph in Figure 5.3 shows how the test was setup in a sand box (Sand's relative permittivity$\epsilon_r \approx 10$), where the antenna is facing the ground with its Teflon layer in full contact with the sand surface. The S11 results (Figure 5.4) show a close correlation between the simulated result, with the operating bandwidth figure comparable to one another. The 10dB band of the measured result (513 - 718MHz) compared to the simulated band (572 - 766MHz) shows that there is an increase in bandwidth and centre frequency, where the mismatches between the two should be from the overall difference in the sand's electrical properties with the simulation input, as well as transmission losses from the balun transformer and the termination resistance. The resonance of the balun transformer is detected at a much higher frequency of 2.9GHz when monitoring S11 using the network analyser.

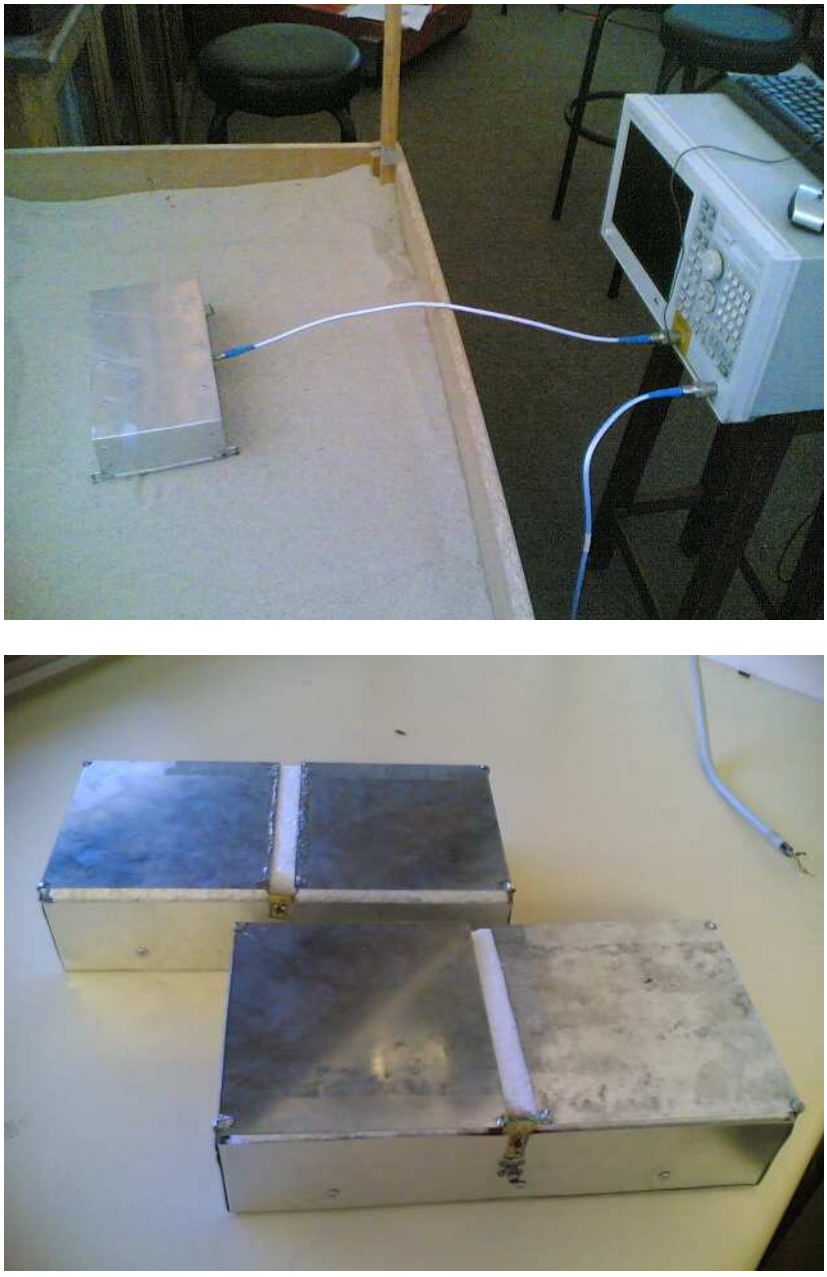

Figure 5.3: Photograph of the antennas and S11 sand box testing arrangement with Agilent E5062A network analyser

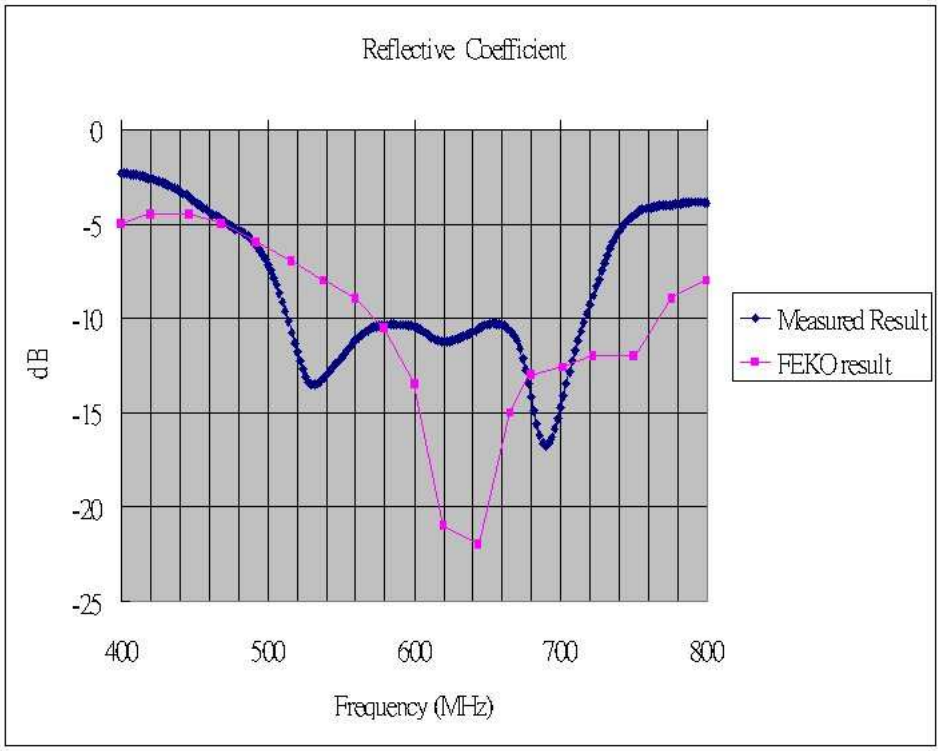

Figure 5.4: Validating the fabricated antenna S11 with the simulated result

5.5 Coupling Analysis

As the GPR antennas will be operating in close range (distance between Tx and Rx antenna) bistatic mode, it is necessary to investigate the cross-coupling between the transmit and receiver antenna. The antennas are placed in three different configurations as shown in Figure 5.5, where the arrows shows the direction of the E field and distance d indicates the edge-to-edge separation between them. With these configurations, it can be seen that configuration 1 and 3 are co-polarised where as 2 is cross-polarised.

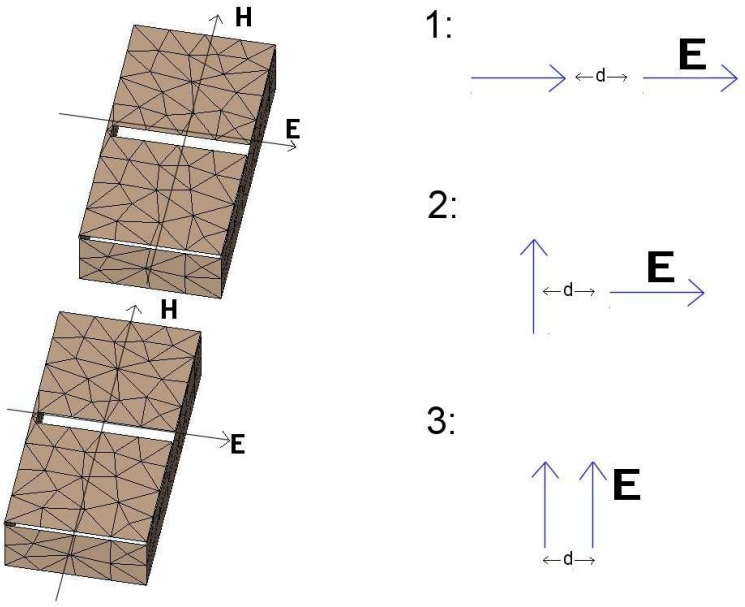

Figure 5.5: Bistatic antenna configurations

From the cross-coupling results shown in Figure 5.6 to 5.9, it can be observed that configuration 3 has the least cross-talk of at least -45 dB of isolation when d is set 10cm and above apart.

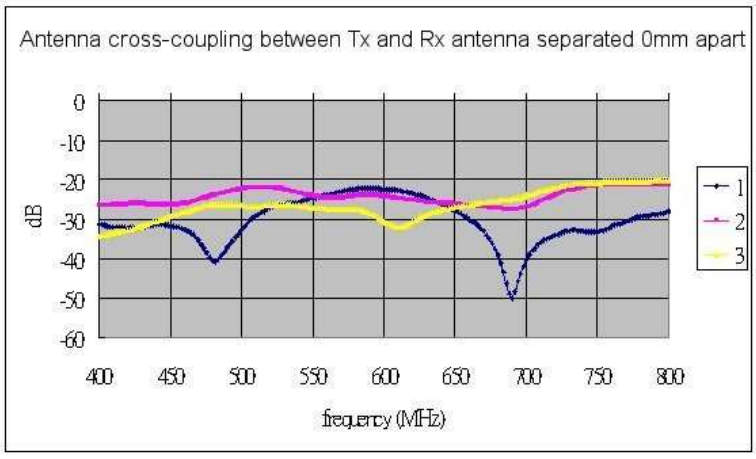

Figure 5.6: Cross-coupling of antennas at 0mm separation

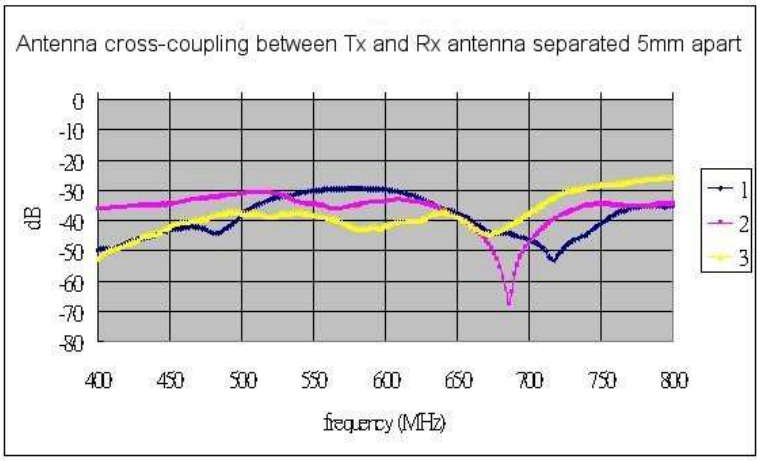

Figure 5.7: Cross-coupling of antennas at 5mm separation

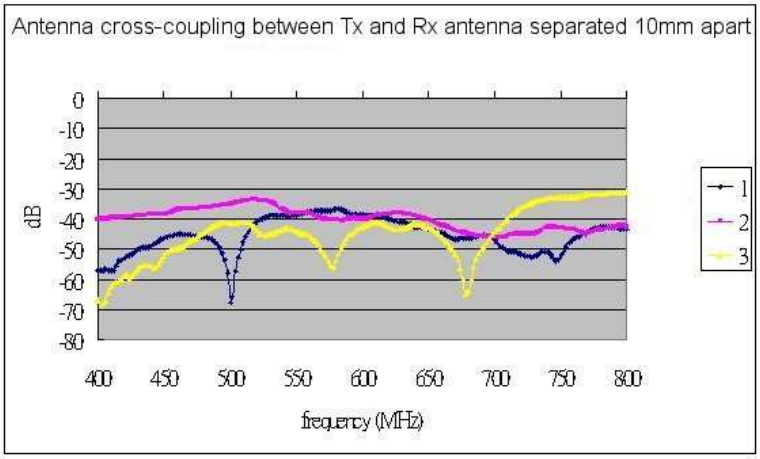

Figure 5.8: Cross-coupling of antennas at 10mm separation

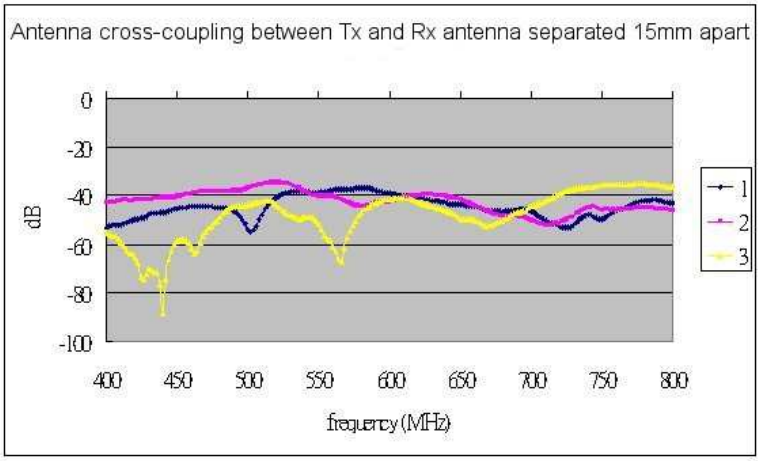

Figure 5.9: Cross-coupling of antenna at 15mm separation

5.6 Object Detection

The final test conducted in this chapter is investigating whether the antennas are capable of object detection. As shown in Figure 5.10, the antennas are placed above a 60x60mm wide metal plate buried 15cm beneath the sand's surface. Due to surface area limitations, only eight samples were taken at 2cm intervals within close proximity above the metal plate. The Tx and Rx antennas are separated 10cm apart implementing configuration 3 (Figure 5.5) defined in the previous section. This setup has proven to have minimal cross-coupling while keeping both antennas at a close proximity to each other. These sampling displacement intervals are illustrated below:

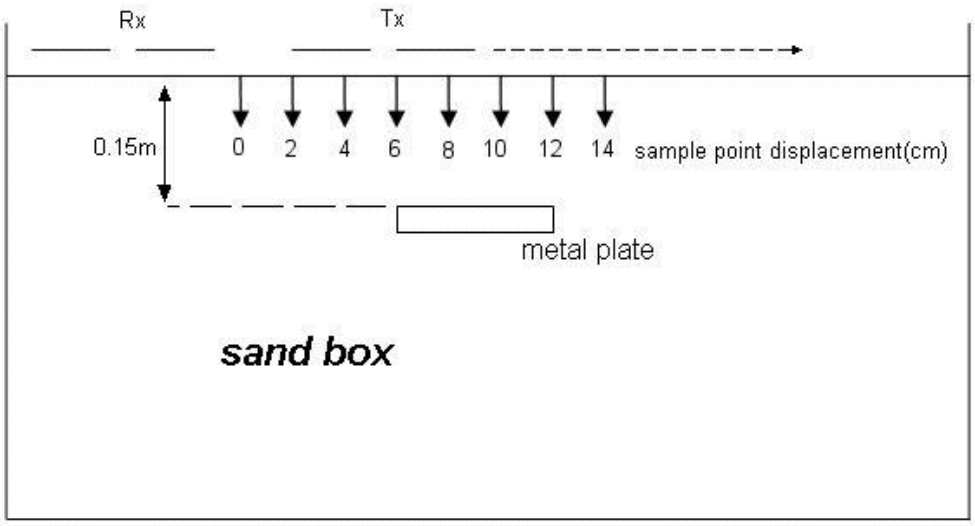

Figure 5.10: Sand box object detection test configuration

S12 insertion loss between the Tx and Rx antennas were taken at each points illustrated in Figure 5.10. The eight sample values are then inverse Fourier transformed to obtain the corresponding time-domain response which are displayed in Figure 5.11, where the y-axis shows the displacement at which the antennas are placed to obtain insertion losses and the x-axis displaying the depth at which response occurs. Due to unknown fix delay in antennas and cables, the depth information is set to be zero from where maximum surface reflections are observed. The results shown correspond to the depth displacement of the buried metal plate where the region labelled "time response" contains the difference in time response signals between the samples. The first three samples have a longer delayed response as the receiver antenna are located further away from the object. The following four equivalent response matches the equal distances travelled between the antennas as it is located right on top of the flat metal plate. The last signal represent the slightly shorter response due to the receiver antenna situated directly on top of the object, hence

less time needed for the signal to travel. There are strong concurrent response detected at shallow depth, observed within the dotted barrier labelled “ground reflections”, this is due to initial sand surface reflections.

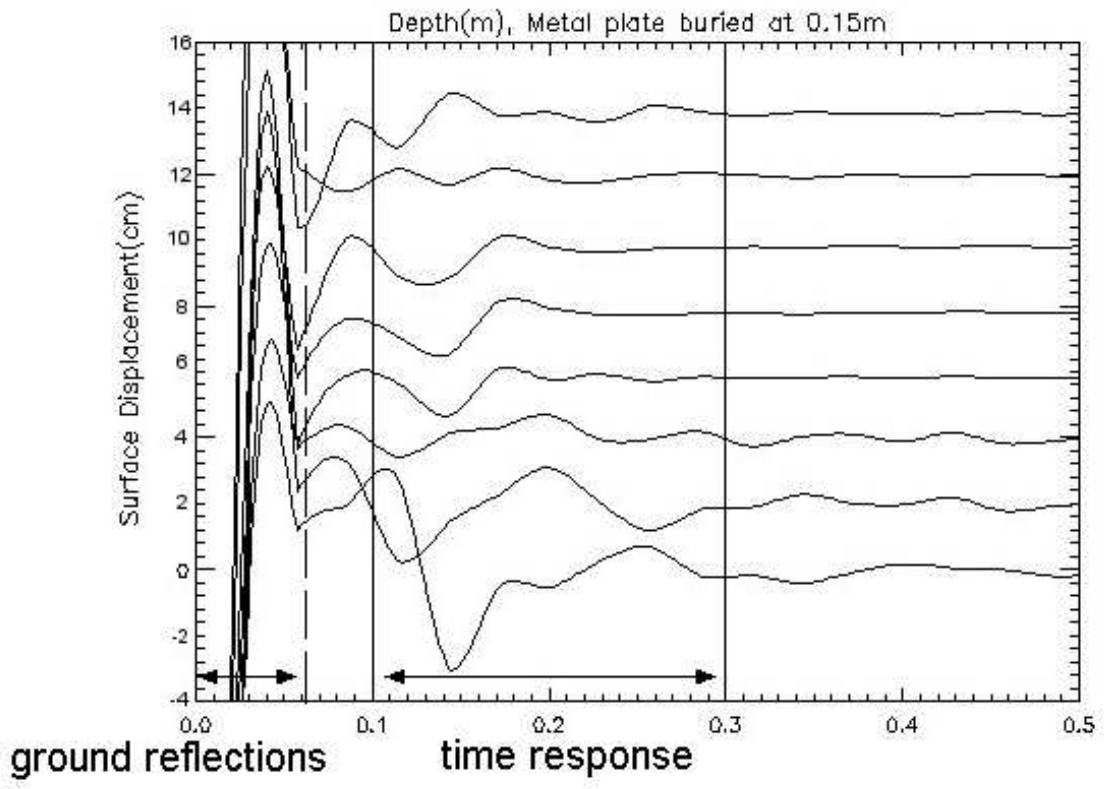

Figure 5.11: Time-domain object detection results of a metal plate buried at a depth of 15cm

5.7 Conclusion

In this chapter, the construction and testing methods of the antenna is shown and discussed. The S11 results obtained from the network analyser shows that although the 10dB band of the measured (513 - 718MHz) and the simulated band (572 -766MHz) shows close correlation, it still has a increase in bandwidth. This is due to the difference in sand’s electrical properties from the simulation input, as well as transmission losses from the balun transformer and the termination resistors. Besides simulation validation, coupling analysis and object detection were also conducted. The results shown in Section 5.5 concludes that Tx and Rx antenna placement implementing configuration 3 (Figure 5.5) will have minimal cross-coupling. The buried metal plate detection experiment using the network analyser has also proven that the antennas are realistically capable of transmitting

and detecting response from objects buried in sand.

Chapter 6

Conclusions and Recommendations

This chapter includes conclusions drawn from the results obtained in Chapters 3, 4 and 5.

6.1 Ground penetration transmitter-receiver time response simulations done in FEKO and FDTD

FEKO's simulation results shows that the MoM planar multilayer Green's function's ability to compute transit time in subsurface layered media has a comparable accuracy to one using FDTD method. Although results from FDTD (Blackman-Harris function point source) simulations seems less cluttered due to less attenuation, implementation of dipole antennas gives a much more realistic result when comparing shapes and duration of waveforms. If only the direct and reflected wave's time response is needed, then FDTD point source simulation have proven to have a less attenuated. Further studies can be conducted on the shape change of receiver waveforms, this will provide a better understanding of subsurface media properties.

6.2 GPR fat dipole modelling

The design and modelling of a 400 - 800MHz ultra wide-band GPR antenna was successfully investigated, fabricated and validated. The fat dipole design have been implemented and modified to the desired operating bandwidth. The following objectives have been met with the improved metallic cased fat dipole design:

- The edge terminations resistors have proven to reduce reflections from lower frequencies hence improving the operating bandwidth.

- Both impedance matching and balun implementation has been resolved by means of a RF transformer, thus reducing the cost and complexity of the antenna.
- The metallic casing of the polystyrene dielectric region has allowed the antenna to achieve the directive half hemisphere radiation pattern required for a GPR application.
- The extremely low permittivity and conductivity of expanded polystyrene dielectric region implemented in this design has proven to have a much improved radiation efficiency over the traditional absorptive GPR antennas. It provides an efficiency of 50% and above from 450MHz onward, where as the absorptive antennas has a trade-off in losing half it efficiency in order to obtain the half hemisphere radiation effect.
- The cross-coupling measurement has shown that when operating these antennas in a GPR application, the transmit and receiver antenna should be placed at a co-polarised position shown in antenna configuration 3 (Figure 5.5). This will provide at least -45dB isolation within the operating bandwidth.
- The object detection experiment conducted has proven that the fat dipole antennas are realistically capable of transmitting and detecting response from objects buried in sand.

This investigation has proven that FEKO is a practical tool for simulating UWB antennas. Its implementation of the multilayer Green's function for computing dielectric substrate has given good indications of how design elements affect the reflection coefficient and efficiency of the antenna.

6.3 Future work

The following GPR experiments can be investigated to improve the antenna's performance:

1. A sandbox with greater surface area can be constructed so that further test in object detection can be done with more sampling intervals to improve result definition.
2. Metal object of different shapes can be buried to compare the change in scattered response.
3. Further GPR Field work, such as the detection of buried pipes and subsurface void, can be done to test the feasibility of the antennas in realistic applications.
4. Different construction methods of this antenna design can be implemented and research into various dielectric materials to improve the robustness of the cased fat dipole.

Appendix A

Software Source Code

A.1 FEKO Code

A.1.1 Subsurface Transit Response - EDITFEKO

This part of the code contains the experimented methods of using dielectric bodies, as well as Green's multi-layer functions, in order to define the sand and clay regions needed for Transit Response simulations.

****** Frequency and wavelength

!!if (not(defined(#freq))) then

#freq = 100.0e6

!!endif

#scaling = 1

#maxfreq = 2e9

#lam = #c0/#maxfreq

********** Define the edge length **********

#edge_len = (2 - #freq/#maxfreq)*#lam/4

** #edge_len = #lam/4

********** Parameters for segmentation**********

#seg_rad = #lam/1000 ** radius of the wire segments\

#seg_len = #lam/20 ** maximum length of wire segments

*******maximum edge length - *Defined for experimentations with dielectric bodies*

** #tri_len = #lam/100

#l = 0.4*#seg_len

IP #seg_rad #seg_len

********** *-Borehole defined for experimentations with dielectric bodies*

** ** Borehole

** DP a 0.032 -0.032 2

** DP b -0.032 -0.032 2

** DP c 0.032 0.032 2

** DP d 0.032 -.032 0

** QU a b c d 1 0 0.00000001

**********- *Sand layer defined for experimentations with dielectric bodies*

** ** Sand Layer

** DP A 1 0 2

** DP B 0 0 2

** DP C 1 2.75 2

** DP D 1 0 0

** LA 1

** QU A B C D 1 0 0.001

**********- *Sand layer defined for experimentations with dielectric bodies*

** Clay Layer

** DP E 1 0 2

** DP F 0.5 0 2

** DP G 1 2.75 2

** DP H 1 0 0

** LA 2

** QU E F G H 40 0.5 1073

**********- *Second sand layer defined for experimentations with dielectric bodies*

** ** Sand Layer

** DP a 0.5 0 1

** DP b 0 0 1

** DP c 0.5 1.375 1

** DP d 0.5 0 0

** LA 1

** QU a b c d 20 0.0001 1800

** ** clay

** DP e 1 0 1

** DP f 0.5 0 1

** DP g 1 1.375 1

** DP h 1 0 0

** LA 2

** QU e f g h 40 0.005 1073

**

** ** SY 1 0 1 1

********** Length defined for Dipole Antennas**********

#U = #lam/4

#D = -#lam/4

#Ul = #l

#Dl =-#l

**********Transmitter**********

DP A 0 0 -#U

DP B 0 0 -#l

DP C 0 0 #l

BL A B

SY 1 0 0 3

LA 1

BL B C

TG 1 0 1 1 0 5.25

*********Receiver Placements**********

** LA 1

```
** BL T3 T4
**
** LA 2
** DP R3 0 4 #Ul
** DP R4 0 4 #Dl
** BL R3 R4
**
** LA 3
** DP T3 0 -1 #Ul
** DP T4 0 -1 #Dl
** DP T5 0 -1 #D
** BL T4 T5
** BL T3 T4
**
** LA 4
** DP R3 0 1 #Ul
** DP R4 0 1 #Dl
** DP R5 0 1 #D
** BL R4 R5
** BL R3 R4
** **********Apply the scaling factor**********
SF 1 #scaling
********** End of geometric input**********
** EG 1 0 0 0 20 0.0001 1073 1
EG 1 0 0 0 1
************************************************************
** Set the frequency
FR 1 #freq
** Excitation
A1 0 1 1 0 50
```

FF 0

** FF 1 1 1 0 90 90 0 0

**********Green’s Function Multi-layer - ground layers (Sand and Clay)**********

GF 12 3 0 2.2

0.2 40 1 0.5

4 20 1 0.0001

0.2 40 1 0.5

** Receiver current

OS 4 2 1

** End

EN

A.1.2 Subsurface Transit Response - TIMEFEKO

** Define the Pulse form

GAUSS

** Parameters of the Gaussian pulse

** Time shift Exponent

10e-9 300e6

FREQUENCY

** Upper frequency Number of Samples

225e6 46

** Normalise the time to that of the speed of light

** NORM

** Output the excitation

EXCITATION

A.1.3 KERI and Microline Co. Ltd Fat Dipole - EDITFEKO

#freq = 300e+6

#lam = 1000*(#c0/#freq)

SF 1 0.001

** #seg_rad = 0.01

** #seg_len = 10

** #tri_len = 10

** IP #seg_rad #tri_len #seg_len

********** Import model BIG dipole**********

IN 8 31 "FD.cfm"

** ** ******* Import model dipole **********

** IN 8 31 "FDs.cfm"

** End of geometry

EG 1 0 0 0 1

** Set frequency

FR 21 0 0.1e+08 4.1e+08

GF 10 2 0 10 1 1e-5 0

1 4.8 1 0

200 1 1 0

** DI Poly 2.3 1 5e-4

** GF 10 1 0 10 1 1e-5 10

** 72.5 2.3 1 5e-4

** SP 50

**********Experimentations of Various Dipole Feed**********

** A4 0 -1 0 1 0 3 1 0

AE: 0 : dipole.feed : dipole.feed1 : 0 : : 1

** AE 0 a b 3 1

** A4 0 -1 1 1 0 0 0 0 0.65

** A4: 0 : Polygon2.Face36 : 0 : : : 1 : : 0 : 0 : 0

** A1: 0 : dipole.feed : : : : 1

OS 2 0

** OF 1 0 0 20 0

** End of file

EN

A.1.4 Improved 400 - 800 MHz Fat Dipole - EDITFEKO

#freq = 300e+6

#lam = 1000*(#c0/#freq)

SF 1 0.001

** #seg_rad = 0.01

** #seg_len = 10

** #tri_len = 10

** IP #seg_rad #tri_len #seg_len

** *****Import model Cased Fat Dipole

IN 8 31 "FD.cfm"

EG 1 0 0 0 1

** Set frequency

FR 21 0 0.1e+08 4.1e+08

GF 10 2 0 10 1 1e-5 0

1 4.8 1 0

200 1 1 0

** DI Poly 2.3 1 5e-4

** GF 10 1 0 10 1 1e-5 10

** 72.5 2.3 1 5e-4

** SP 50

********** Set Source and Experimentation Excitations**********

** A4 0 -1 0 1 0 3 1 0

AE: 0 : dipole.feed : dipole.feed1 : 0 : : 1

** AE 0 a b 3 1

** A4 0 -1 1 1 0 0 0 0 0.65

** A4: 0 : Polygon2.Face36 : 0 : : : 1 : : 0 : 0 : 0

** A1: 0 : dipole.feed : : : : 1

OS 2 0

** OF 1 0 0 20 0

** End of file

EN

A.2 IDL Code

IDL code was used to display the time-domain result calculated by TIMEFEKO

A.2.1 Subsurface Time Response - Graphical Display

```
;————————Antenna Distance 2m————-
filename = "ground2m.aus"
header1 = strarr(12+128+8+128+7) ;283
array1 = fltarr(4,128) ;4
header2 = strarr(6) ;6
array2 = fltarr(2,128) ;2
openr, lun, filename, /get_lun
readf, lun, header1, array1, header2, array2
close,lun
Xaxis1 = array1[0,*]
Yaxis1 = array1[3,*] ;3
Xaxis2 = array2[0,*]
Yaxis2 = array2[1,*]
fx = findgen(n_elements(Xaxis1))
gx = findgen(n_elements(Xaxis1)*10)/10
fy = findgen(n_elements(Yaxis1))
gy = findgen(n_elements(Yaxis1)*10)/10
curve1x = (interpol(Xaxis1, fx, gx))/1e-9 ;Interpolation
curve2x = (interpol(Xaxis2, fx, gx))/1e-9 ;Interpolation
curve1y = (interpol(Yaxis1, fy, gy, /spline))/1.5e-8 ;Interpolation
curve2y = (interpol(Yaxis2, fy, gy, /spline))/1.43e-5 ;Interpolation
;————————Antenna Distance 4m—————
filename = "ground4m.aus"
header3 = strarr(12+128+8+128+7) ;283
array3 = fltarr(4,128) ;4
```

```
header4 = strarr(6) ;6
array4 = fltarr(2,128) ;2
openr, lun, filename, /get_lun
readf, lun, header3, array3, header4, array4
close,lun
Xaxis3 = array3[0,*]
Yaxis3 = array3[3,*] ;3
Xaxis4 = array4[0,*]
Yaxis4 = array4[1,*]
fx = findgen(n_elements(Xaxis3))
gx = findgen(n_elements(Xaxis3)*10)/10
fy = findgen(n_elements(Yaxis3))
gy = findgen(n_elements(Yaxis3)*10)/10
curve3x = (interpol(Xaxis3, fx, gx))/1e-9 ;Interpolation
curve4x = (interpol(Xaxis4, fx, gx))/1e-9 ;Interpolation
curve3y = (interpol(Yaxis3, fy, gy, /spline))/1.3e-8 ;Interpolation
curve4y = (interpol(Yaxis4, fy, gy, /spline))/1.43e-5 ;Interpolation
;————————Antenna Distance 5.25m————————
filename = "ground5m.aus"
header5 = strarr(12+128+8+128+7) ;283
array5 = fltarr(4,128) ;4
header6 = strarr(6) ;6
array6 = fltarr(2,128) ;2
openr, lun, filename, /get_lun
readf, lun, header5, array5, header6, array6
close,lun
Xaxis5 = array5[0,*]
Yaxis5 = array5[3,*] ;3
Xaxis6 = array6[0,*]
Yaxis6 = array6[1,*]
```

```
fx = findgen(n_elements(Xaxis5))
gx = findgen(n_elements(Xaxis5)*10)/10
fy = findgen(n_elements(Yaxis5))
gy = findgen(n_elements(Yaxis5)*10)/10
curve5x = (interpol(Xaxis5, fx, gx))/1e-9 ;Interpolation
curve6x = (interpol(Xaxis6, fx, gx))/1e-9 ;Interpolation
curve5y = (interpol(Yaxis5, fy, gy, /spline))/1.3e-8 ;Interpolation
curve6y = (interpol(Yaxis6, fy, gy, /spline))/1.43e-5 ;Interpolation
;————FDTD Import————
aa = fltarr(3,1300)
openr,1,'nbor_Ez_h4_x246.dat'
readu,1,aa
close,1
time = fltarr(1300)
openr,1,'time.dat'
readu,1,time
close,1
;————plot————
!p.multi = [0,1,3]
plot, curve1x, curve1y
oplot,time,(aa(0,*)/1e-4), linestyle = 3
plot, curve3x, curve3y
oplot,time,(aa(1,*)/1e-4), linestyle = 3
plot, curve5x, curve5y
oplot,time,(aa(2,*)/1e-4), linestyle = 3
currdevice=!D.NAME
set_plot,'ps'
device, filename = 'combination.eps', /encapsulated, preview=2, xsize=6, ysize=4.5,/inches
!p.multi = [0,1,3]
plot, curve1x, curve1y, title = 'Time[ns] ____ FEKO —- FDTD 2m' ;Plot label
```

```
oplot,time,(aa(0,*)/1e-4), linestyle = 1
plot, curve3x, curve3y, title = ’ 4m’
oplot,time,(aa(1,*)/1e-4), linestyle = 1
plot, curve5x, curve5y, title = ’ 5.25m’
oplot,time,(aa(2,*)/1e-4), linestyle = 1
device, /close
set_plot, currdevice
currdevice=!D.NAME
set_plot,’ps’
device, filename = ’receiverFDTD.eps’, /encapsulated, preview=2, xsize=3.4, ysize=4,/inches
;Encapsulating the result.
plot,time,(aa(0,*)/1e-4), title = ’FDTD Time[ns] 2m’
plot,time,(aa(1,*)/1e-4), title = ’ 4m’
plot,time,(aa(2,*)/1e-4), title = ’ 5.25m’
device, /close
set_plot, currdevice
end
```

A.2.2 Object Detection

; These are the code used to display the object detection results obained by the Agilent E5062A network analyser.

```
;————————-Data Extraction————————
num_freq = 200
S12_data = dblarr(10, num_freq)
;filename = ’S12_object_detection.txt’
filename = ’try.txt’
openr, u_file,filename,/Get_Lun
readf,u_file,S12_data
free_lun,u_file
freq = reform(s12_data(0,*))
```

```
xpos_0 = reform(s12_data(1,*))
useless = reform(s12_data(2,*))
xpos_2 = reform(s12_data(3,*))
xpos_4 = reform(s12_data(4,*))
xpos_6 = reform(s12_data(5,*))
xpos_8 = reform(s12_data(6,*))
xpos_10 = reform(s12_data(7,*))
xpos_12 = reform(s12_data(8,*))
xpos_14 = reform(s12_data(9,*))
;————Data Plot————————
fs = 800e6
dt = 1/fs
t = findgen(200)*dt
df = (fs/(num_freq))+400e6
ddt = 1/df
tt = findgen(200)*ddt
dsp = tt*(3e8)/(3.16)
td = (1/(freq))
tdd = findgen(200)*td
;dist = td*3e8/3.16
dist =findgen(200)/35
x1 = fft(xpos_0,-1)
x2 = fft(xpos_2,-1)
x3 = fft(xpos_4,-1)
x4 = fft(xpos_6,-1)
x5 = fft(xpos_8,-1)
x6 = fft(xpos_10,-1)
x7 = fft(xpos_12,-1)
x8 = fft(xpos_14,-1)
F1 = findgen(n_elements(x1))
```

```
F1i = findgen(n_elements(x1)*10)/10
F2 = findgen(n_elements(x2))
F2i = findgen(n_elements(x2)*10)/10
F3 = findgen(n_elements(x3))
F3i = findgen(n_elements(x3)*10)/10
F4 = findgen(n_elements(x4))
F4i = findgen(n_elements(x4)*10)/10
F5 = findgen(n_elements(x5))
F5i = findgen(n_elements(x5)*10)/10
F6 = findgen(n_elements(x6))
F6i = findgen(n_elements(x6)*10)/10
F7 = findgen(n_elements(x7))
F7i = findgen(n_elements(x7)*10)/10
F8 = findgen(n_elements(x8))
F8i = findgen(n_elements(x8)*10)/10
Fd = findgen(n_elements(dist))
Fdi = findgen(n_elements(dist)*10)/10
curve1x = (interpol(x1, f1, f1i, /spline)) ;Interpolation
curve2x = (interpol(x2, f2, f2i, /spline)) ;Interpolation
curve3x = (interpol(x3, f3, f3i, /spline)) ;Interpolation
curve4x = (interpol(x4, f4, f4i, /spline)) ;Interpolation
curve5x = (interpol(x5, f5, f5i, /spline)) ;Interpolation
curve6x = (interpol(x6, f6, f6i, /spline)) ;Interpolation
curve7x = (interpol(x7, f7, f7i, /spline)) ;Interpolation
curve8x = (interpol(x8, f8, f8i, /spline)) ;Interpolation
curvedist = (interpol(dist, fd, fdi));Interpolation
plot, curvedist, (curve1x), xrange = [0, 0.5], yrange = [-a, 38*a], title = 'Depth(m)'
oplot, curvedist, (curve2x + a*5)
oplot, curvedist, (curve3x + a*10)
oplot, curvedist, (curve4x + a*15)
```

```
oplot, curvedist, (curve5x + a*20)
oplot, curvedist, (curve6x + a*25)
oplot, curvedist, (curve7x + a*30)
oplot, curvedist, (curve8x + a*35)
end
```

Appendix B

TC4-1W Balun Transformer Data Sheet

Surface Mount

RF Transformer

TC4-1W+

50Ω 3 to 800 MHz

CASE STYLE: AT224-1
PRICE: $1.19 ea. QTY (100)

+ RoHS compliant in accordance with EU Directive (2002/95/EC)

The +suffix has been added in order to identify RoHS Compliance. There has been no change to the model's material, form, fit, or function. See our web site for RoHS Compliance methodologies and qualifications.

Maximum Ratings

Operating Temperature	-20°C to 85°C
Storage Temperature	-55°C to 100°C
RF Power	0.25W
DC Current	30mA

Pin Connections

PRIMARY DOT	6
PRIMARY	4
SECONDARY DOT	1
SECONDARY	3
SECONDARY CT	2
NOT USED	5

Features

- wideband, 3-800 MHz
- good return loss
- aqueous washable

Applications

- impedance matching
- push-pull amplifiers

Outline Drawing AT224-1

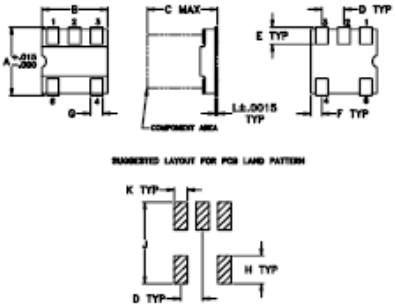

Outline Dimensions (inch / mm)

A	B	C	D	E	F
.150	.150	.160	.050	.040	.025
3.81	3.81	4.06	1.27	1.02	0.64

G	H	J	K	L	wt
.028	.065	.190	.030	.007	grams
0.71	1.65	4.83	0.76	0.18	0.15

Config. A

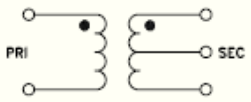

Transformer Electrical Specifications

MODEL NO.	Ω RATIO	FREQUENCY (MHz)	INSERTION LOSS*		
			3 dB MHz	2 dB MHz	1 dB MHz
TC4-1W+	4	3-800	3-800	5-400	10-100

* Insertion Loss is referenced to mid-band loss, 0.8 dB typ.

Typical Performance Data

FREQUENCY (MHz)	INSERTION LOSS (dB)	INPUT R. LOSS (dB)
3.00	1.09	11.58
4.00	0.98	12.35
5.00	0.93	13.11
7.50	0.86	14.21
10.00	0.83	14.49
100.00	0.88	15.77
250.00	0.96	16.17
400.00	1.13	16.72
600.00	1.36	15.59
800.00	2.21	9.07

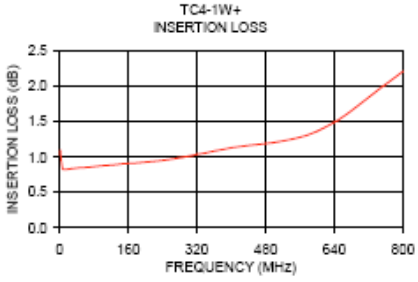

Bibliography

[1] GeoModel, “Ground Penetrating Radar Basic Operating Principals”, *www.geomodel.com/gprtext.htm, GeoModel, Inc.* March 2005.

[2] Saul Rodriguez Duenas, “Ultra Wide Band Systems”, *www.imit.kth.se/courses/2B1457/Lecture05/lecture7_UWB_lecture_Saul.pdf, KTH*,2005 .

[3] Mathworld, “Green’s Function”, *mathworld.wolfram.com/GreensFunction.html, WOLFRAM RESEARCH*, September 2004.

[4] NI Developer Zone, “Windowing: Optimizing FFTs Using Window Functions”, *National Instruments*, June 2005.

[5] R. Clarke, R. Karunaratni, C. Schrader, “Ultra-Wide Band Antenna”, *College of Engineering, San Jose State University.* Fall 2004.

[6] EM Software & Systems-S.A. (Pty) Ltd, “FEKO User’s Manual”, *FEKO 48.294, PREFEKO 27.55-60 and later*, June 2004.

[7] K.P. Mudhopadhyay, M.R. Inggs and A.J. Wilkinson, “FTDT Modelling of a Borehole Radar Wave Propagation: a 3-D Simulation Study in a Conductive Media”, *International Geoscience and Remote Sensing Symposium*, pp 109–126, 2005.

[8] K.P. Mudhopadhyay, “Three-Dimensional Finite Difference Time Domain Modelling of Borehole Radar in mining applications”, *Radar and Remote Sensing Group, Department of Electrical Engineering, University of Cape Town, South Africa*, 2004.

[9] P.W Futter, “Advance Modelling of a Borehole Radar Environment with the FDTD Method”, *Matieland, South Africa, Stellenbosch University*, 2001.

[10] Guy Atkin, “T2FD–The Forgotten Antenna”, *www.hard-core-dx.com/nordicdx/antenna/wire/t2fd.html, HCDX Antennas*, April 2002.

[11] Max Birch, “Development of a Cavity Backed Bowtie Antenna with Dielectric Matching for Ground Penetrating Radar”, *Matieland, South Africa, University of Stellenbosch,* September 2001

[12] Alex Peeters, “Transmission Line Theory”, *www.citap.com/documents/tcp-ip/tcpip021.htm, TCI-IP Networks,* March 2003.

[13] Enrico M. Staderini, “A Pratical Imtroduction to Ultra Wideband Technology”, *Tor Vergata University of Rome*, 2004

[14] Korea Electrotechnology Research Institute (KERI) & Microline Co., Ltd., “Buried Small Object Detected by UWB GPR”, *Proc. of Asia Pacific Microwave Conference 2003 (APMC’03)*, 2003

[15] D. Jeffrereys, “www.ee.surrey.ac.uk/Personal/D.Jeffreys/mmethod.html”, *Technical report, University of Surrey*, 2004

[16] Seok H Choi, Jong K. Park, Sun K. Kim and Jae Y. Park, “A New Ultra-Wideband Antenna For UWB Applications”, *Department of Radio Wave Engineering, Hanbat National University*, August 2003

[17] J. Silvertrim, “IEEE Ultra wideband Presentation”, *Innovative Wireless Technologies, 1047 Vista Park Drive Suite A, Forest,* October 2003

[18] David Kinnon, “Identification of Land Mine using Microwave Resonance Signature”, *University of Queensland*, October 1999

[19] A.A Lestari, A.G Yarovoy, L.P. Ligthart, “Capacitively-Tapered Bowtie Antenna”, *International Research Center for Telecommunications-Transmision and Radar, Delft University of Technology, Faculty of Information Technology and Systems*, 2003

[20] A.G Yarovoy, L.P. Lighart, “Ultra-Wideband Antennas for Ground Penetrating Radar”, *International Research Center for Telecommunications-Transmision and Radar, Delft University of Technology, Faculty of Information Technology and Systems*, 2003

[21] A.G Yarovoy, P.J. Aubrey, L.P. Lighart, “GPR Antenna Measurements in Time Domain”, *International Research Center for Telecommunications-Transmision and Radar, Delft University of Technology, Faculty of Information Technology and Systems*, 2003

[22] Hans Gregory Schantz, “Radiation Efficiency of UWB Antennas”, *Proceedings of the 2002 IEEE UWBST Conference, 2002.*

[23] D.M. Pozar, ”Microwave and RD Design of Wireless Systems”, *John Wiley and Sons*, 2001